

# Boosting Column Generation with Graph Neural Networks for Joint Rider Trip Planning and Crew Shift Scheduling

Jiawei Lu, Tinghan Ye\*, Wenbo Chen, and Pascal Van Hentenryck

H. Milton Stewart School of Industrial & Systems Engineering,  
Georgia Institute of Technology, Atlanta, GA

## Abstract

Optimizing service schedules is pivotal to the reliable, efficient, and inclusive on-demand mobility. This pressing challenge is further exacerbated by the increasing needs of an aging population, the over-subscription of existing services, and the lack of effective solution methods. This study addresses the intricacies of service scheduling, by jointly optimizing rider trip planning and crew scheduling for a complex dynamic mobility service. The resulting optimization problems are extremely challenging computationally for state-of-the-art methods.

To address this fundamental gap, this paper introduces the Joint Rider Trip Planning and Crew Shift Scheduling Problem (JRTPCSSP) and a novel solution method, called Attention and Gated GNN-Informed Column Generation (AGGNNI-CG), that hybridizes column generation and machine learning to obtain near-optimal solutions to the JRTPCSSP with real-life constraints of the application. The key idea of the machine-learning component is to dramatically reduce the number of paths to explore in the pricing problem, accelerating the most time-consuming component of the column generation. The machine learning component is a graph neural network with an attention mechanism and a gated architecture, which is particularly suited to cater for the different input sizes coming from daily operations.

AGGNNI-CG has been applied to a challenging, real-world dataset from the Paratransit system of Chatham County in Georgia. It produces substantial improvements compared to the baseline column generation approach, which typically cannot produce high-quality feasible solutions in reasonable time on large-scale complex instances. AGGNNI-CG also produces significant improvements in service quality compared to the existing system.

**Keywords:** *Service Scheduling, Paratransit, Column Generation, Graph Neural Network*

---

\*Corresponding author: [joe.ye@gatech.edu](mailto:joe.ye@gatech.edu)

# 1 Introduction

Improving the efficiency, accessibility, and reliability of transportation service scheduling is a vital challenge in both academic research and practical applications. The increasing complexities of urban mobility, driven by growing traffic congestion, the environmental impact of private vehicles, and the operational rigidity of traditional transit systems, demand innovative solutions. Additionally, as the population ages and the demand for accessible transportation services rises, there is an urgent need to optimize how mobility services are scheduled and delivered.

Transportation service scheduling plays a pivotal role in ensuring that diverse rider needs are met efficiently. From managing public transit networks to coordinating on-demand services, effective scheduling is essential for improving operational efficiency and user satisfaction. The challenge becomes even more significant when accounting for dynamic real-world conditions such as fluctuating demand, variable travel times, and resource constraints, all of which can hinder the performance of traditional scheduling methods.

As another example, Paratransit services, designed to serve riders with disabilities or those unable to access regular transit, provide a compelling case for the complexities involved in transportation service scheduling. These systems often experience oversubscription due to the increasing needs of an aging population, coupled with limited operational resources. This situation underscores the importance of optimizing schedules to balance service quality with operational costs.

## 1.1 Motivations and Contributions

The scheduling in these diverse transportation systems — whether in traditional transit, on-demand services, or specialized Paratransit operations — is a multifaceted challenge. Despite notable progress in service scheduling, several key challenges still require significantly more attention. First, there is a discernible need for an integrated framework that simultaneously addresses *rider trip plans* and *crew shift scheduling*. To date, within the academic sphere and in practice, these elements are predominantly examined in isolation, highlighting the necessity for a more holistic approach. Second, the inherent complexity of such an integrated problem in transportation systems poses significant computational challenges. This complexity arises from the need to jointly optimize intricate rider trip itineraries (often involving multiple requests per rider) alongside dynamically determining optimal crew shifts within maximum working hour limits, unlike many traditional routing problems with predefined schedules. Third, evaluating solution methods often relies on synthesized datasets, leaving a void in capturing the realities encountered in the field. Particularly, these realities include complex and fluctuating demand patterns — regarding spatial-temporal distributions and correlations between a rider's multiple requests — factors that synthetic data often struggle to fully replicate, thereby impacting algorithm performance evaluation.

This study aims at addressing these challenges by introducing an integrated approach for the Joint Rider Trip Planning and Crew Shift Scheduling Problem (JRTPCSSP) for mobility systems. Moreover, to address the computational challenges of the JRTPCSSP, the study combines a traditional column generation with an Attention-Based, Gated Graph Neural Network to reduce the search space and find high-quality solutions quickly. More precisely, the primary contributions of this research can be summarized as follows:

- Problem Formulation: This study formally defines and characterizes the JRTPCSSP, explicitly capturing the joint optimization of rider trip planning and crew shift scheduling with relevant real-world constraints, highlighting its complexities compared to related but distinct routing and scheduling problems.

- Efficient Solution Method: This study proposes Attention and Gated GNN-Informed Column Generation (AGGNNI-CG), a method that synergistically integrates column generation with a purpose-built Graph Neural Network (GNN). The core idea is to leverage the GNN to effectively learn complex patterns from the JRTPCSSP pricing problem’s structure and constraints, thereby drastically reducing the search space by predicting the most promising paths (columns) to explore.
- Tailored GNN Architecture: This study designs a specific GNN architecture incorporating attention mechanisms and gated units. This architecture is motivated by the need to effectively process the graph-structured pricing problem inherent in JRTPCSSP and handle varying input sizes typical of daily operations. Unlike existing approaches that rely on local edge-level predictions or maintain computationally expensive edge embeddings, the proposed model integrates edge features directly into the attention weight calculations, eliminating memory bottlenecks while preserving representational power. This architectural innovation enables application to large-scale real-world instances and enhances edge classification performance.
- Validation on Real-World, Large-Scale Instances: This study evaluates the proposed AGGNNI-CG method through extensive computational experiments using large-scale instances derived directly from real-world operational data. This evaluation strategy is crucial, as the performance of machine learning models can be sensitive to the characteristics of the input data; results on synthetic instances may not fully reflect performance on operational challenges where demand patterns are complex and not easily replicated.

## 1.2 Related Work

### 1.2.1 Service Scheduling in Transportation Systems

Service scheduling in transportation systems involves coordinating both the rider and crew aspects. This includes rider trip plan scheduling and crew shift scheduling, both of which have been widely studied in the literature due to their critical role in real-world operations.

For rider trip plan scheduling, the objective is to generate an optimal travel plan that fulfill the travel needs of a rider from origin to destination. A travel plan may consist of multiple travel segments, each of which is specified by travel mode, departure time, arrival time, and other information. Of course, rider trip requests are fulfilled by drivers/vehicles, especially in on-demand transportation systems. Therefore, trip plan scheduling is highly correlated with driver/vehicle tasks, i.e., at what time to serve which riders in what order. In the literature, the type of problem is typically modeled as Dial-A-Ride Problem (DARP), which is a variant of the general vehicle routing problem. Readers are referred to for a comprehensive review of the DARP by [Cordeau and Laporte \(2007\)](#) and [Ho et al. \(2018\)](#). Solution methods in the existing studies can be classified into two classes: exact methods such as branch-and-cut ([Cordeau, 2006](#); [Ropke et al., 2007](#)), branch-and-price ([Garaix et al., 2010, 2011](#)), and branch-and-price-and-cut algorithm ([Qu and Bard, 2015](#); [Gschwind and Irnich, 2015](#)); heuristics such as tabu search ([Cordeau and Laporte, 2003](#); [Kirchler and Calvo, 2013](#)), simulated annealing ([Braekers et al., 2014](#)), large neighborhood search ([Ropke and Pisinger, 2006](#); [Jain and Hentenryck, 2011](#); [Gschwind and Drexel, 2019](#)), and genetic algorithm ([Jorgensen et al., 2007](#); [Cubillos et al., 2009](#)). In general, exact methods take longer time to produce high-quality solutions with bound information, while heuristics usually generate relatively good solutions without bound information within

a shorter time. In the literature, most studies use either exact methods or heuristics; few study combines exact methods and heuristics in solving DARP.

For crew shift scheduling in public transit systems, a key challenge is the driver shift scheduling, whose objective is to design optimal driver shifts based on driver availability and time-varying rider travel needs in such a way that supply and demand are matched over time. The literature on driver scheduling in public transportation systems primarily focuses on traditional fixed-route systems (e.g., buses) and several key areas of research and methodological developments. Notable studies include exploring genetic algorithms for shift construction (Wren and Wren, 1995), defining efficient driver scheduling methodologies (Tóth and Krész, 2013), and integrating vehicle and crew scheduling with driver reliability (Andrade-Michel et al., 2021). Further research delves into robust and cost-efficient resource allocation for vehicle and crew scheduling, addressing operational disruptions (Amberg et al., 2019), and developing new mathematical models for the Drivers Scheduling Problem (DSP) that accurately reflect real-world complexities (Portugal et al., 2009). Studies also extend to addressing scheduling problems with mealtime windows and employing Integer Linear Programming (ILP) models for effective scheduling (Kang et al., 2019), and integrating duty scheduling and rostering to enhance driver satisfaction in public transit (Borndörfer et al., 2017). However, there is a notable gap in research focusing on emerging on-demand transit systems, as most studies primarily concentrate on conventional fixed-route bus systems, leaving room for exploration in the context of modern, demand-responsive transport models.

### 1.2.2 Machine Learning for Combinatorial Optimization

The integration of machine learning techniques to address combinatorial optimization problems has become an increasingly prominent field of study in recent years. Interested readers can refer to comprehensive reviews of recent progress by Bengio et al. (2021), Kotary et al. (2021), Mazyavkina et al. (2021), and Karimi-Mamaghan et al. (2022). Research endeavors in this domain generally fall into one of the two categories: the application of standalone machine learning models to derive solutions for combinatorial problems and the enhancement of traditional mathematical optimization methods through machine learning.

In the first category, deep learning-based neural network architectures are typically designed to identify patterns that connect problem instances to their optimal solutions. This process may involve learning from a dataset of existing solutions — a supervised learning approach (e.g., Vinyals et al. (2015)) — or discovering strategies through a process of trial and error, akin to reinforcement learning (e.g., Nazari et al. (2018)) or both as in Yuan et al. (2022a). The goal is to train machine learning models in a sufficiently robust manner to generate solutions autonomously. Despite the progress, achieving high-quality solutions solely with machine learning remains a challenging frontier. Combinatorial optimization problems are inherently complex and encompass vast solution spaces that are difficult to navigate efficiently. As a result, while machine learning models have shown promise, they often struggle to match the solution quality of established optimization methods. Recent studies underscore the persistent difficulty in bridging this quality gap, suggesting the need for more sophisticated models and training techniques.

In the latter category, machine learning models, once adequately trained, are often employed to streamline or assist with the most time-intensive aspects of traditional mathematical optimization methods. This can involve pivotal tasks such as choosing cutting planes in branch-and-cut algorithms or selecting columns in branch-and-price algorithms. By synergizing the strengths of both mathematical optimization and machine learning, this hybrid approach has demonstrated considerable promise in tackling a range of complex problems. Specifically, in the realm of enhancing the column generation algorithm through machine learning

techniques - a critical component in vehicle routing and service scheduling within transportation systems - researchers have recorded notable advancements. [Morabit et al. \(2021\)](#) applied a learned model to select promising columns from those generated at each iteration of column generation to reduce the computing time of reoptimizing the restricted master problem. [Shen et al. \(2022\)](#) designed an ML model to predict the optimal solution of pricing subproblems, which is then used to guide a sampling method to efficiently generate high-quality columns.

Further advances in this field involve using machine learning to streamline pricing subproblems. Pioneering studies have employed machine learning techniques to simplify underlying graphs, thereby lessening the complexity of these subproblems. [Morabit et al. \(2023\)](#) utilized a random forest model to predict edges likely to be part of the master problem's solutions. Owing to the complexity and variable sizes of the graphs in subproblems, their model bases its predictions on local rather than global graph information. In addressing varying graph sizes, [Yuan et al. \(2022b\)](#) developed a graph neural network model with residual gated graph convolutional layers, inspired by [Joshi et al. \(2019\)](#). Their model evaluates the likelihood of each edge being part of the final solution, leading to the construction of a reduced graph that retains edges with higher predicted probabilities for pricing subproblems. The method proposed in this paper differs from [Yuan et al. \(2022b\)](#) in three key ways: First, this study tackle both crew shift scheduling and rider trip planning, unlike [Yuan et al. \(2022b\)](#) which focused only on the former. Second, the proposed method is applied to considerably larger and more complex real-world scenarios, whereas [Yuan et al. \(2022b\)](#) tested their algorithm on instances of smaller scales. Third, contrary to [Yuan et al. \(2022b\)](#), the proposed architecture in this paper avoids updating the edge embeddings in each layer, a process that is computationally inefficient and leads to prohibitive memory consumption at larger scales during training. Instead, the proposed model integrates graph attention and residual gating mechanisms, incorporating edge-level features in the attention weight calculations without the need to keep track of the edge embeddings. This reduces the risk of memory overload and improves scalability.

### 1.3 Outline of the Paper

The rest of this paper is organized as follows. Section 2 defines the JRPCSSP. Section 3 presents the column generation algorithm. Section 4 describes the machine learning methodology and its integration within the column generation method. Section 5 reports the benefits of the proposed approach on the real-world dataset. Section 6 concludes the paper and discusses future research directions.

## 2 Joint Rider Trip Planning and Crew Shift Scheduling

### 2.1 Problem Description

The JRPCSSP considered in this paper is a variant of the Dial-A-Ride Problem (DARP). Compared to the classic DARP, the JRPCSSP introduces two additional features. First, it considers scenarios where a single rider may have multiple trip requests in a day and imposes a complete service constraint: either all of the rider requests are fulfilled, or none at all. This approach, which disallows partial servicing, is motivated by the need to guarantee return trips (e.g., for dialysis patients). Second, the JRPCSSP enforces a maximum working duration for each driver (e.g., 8 hours), but does not predefine driver shifts. The JRPCSSP assumes a one-to-one correspondence between drivers and vehicles, which reflects realistic scenarios in practice. For ease of notation, the terms “driver” and “vehicle” are used interchangeably throughout the paper.

Formally, the problem is defined as follows. Consider a set of riders  $U$ , with each rider  $u \in U$  associated with a set of trip requests  $R_u$ . These requests are to be accommodated by a homogeneous fleet of vehicles, denoted by  $F$ . Each trip request  $r$  in  $R_u$  has an origin, a destination, and strict time windows for both departure and arrival times. Although fulfilling every trip request is not mandatory, it is crucial to note that partial servicing of a rider requests is not allowed: either all requests in  $R_u$  are served or none of them. The complete set of trip requests from all riders is denoted as  $R = \bigcup_{u \in U} R_u$ . Each vehicle  $f$  in the fleet  $F$  has a capacity of  $C$ , and the fleet size is constant at  $|F|$ . The working shifts of these vehicles are not predefined; instead, they need to be strategically determined alongside the scheduling of the trip requests. The earliest shift start time and latest shift end time are  $\xi_s$  and  $\xi_e$ , respectively. The maximum number of working hours of each vehicle is denoted by  $\eta$ . All vehicles begin and end their service at a common depot. The travel times between the depot, origins, and destinations are known and constant. The primary goal is to design an optimal schedule for the vehicle working hours and the service of trip requests that maximizes the number of requests served. This objective is motivated by a real system in the field, where the number of requests often exceeds the capacity of the service.

Notations used in this section are provided in Table 1.

Table 1: Summary of Notation

| Symbol                    | Description  |
|---------------------------|--|
| <b>Sets</b>               |  |
| $U$                       | Set of riders  |
| $R_u$                     | Set of trip requests for rider $u \in U$   |
| $R$                       | Set of all trip requests, $R = \bigcup_{u \in U} R_u$  |
| $F$                       | Set of homogeneous vehicles  |
| $P/D$                     | Set of pickup/drop-off nodes, one for each request $r \in R$                                     |
| $P_u$                     | Set of pickup nodes associated with rider $u \in U$  |
| $N$                       | Set of nodes in the graph $g$ for the arc-based model; $N = \{0\} \cup P \cup D \cup \{2n + 1\}$ |
| $E$                       | Set of edges in the graph $g = (N, E)$   |
| $\Omega$                  | Set of feasible vehicle routes (paths)   |
| <b>Parameters</b>         |  |
| $n$                       | Total number of trip requests; $n =  R $   |
| $C$                       | Capacity of each vehicle   |
| $\xi_s/\xi_e$             | The earliest shift start time / latest shift end time  |
| $\eta$                    | Maximum working duration (in hours) for each vehicle/driver                                      |
| $d_i$                     | Demand at node $i \in N$ ; $d_i > 0$ for pickup, $d_i < 0$ for drop-off, $d_0 = d_{2n+1} = 0$    |
| $s_i$                     | Service time required at node $i \in N$  |
| $[a_i, b_i]$              | Time window (earliest/latest service start time) for node $i \in N$                              |
| $t_{ij}$                  | Travel time between node $i$ and node $j$ for $(i, j) \in E$                                     |
| $\alpha_{r\theta}$        | Binary parameter: 1 if request $r$ is served by route $\theta \in \Omega$ , 0 otherwise          |
| <b>Decision Variables</b> |  |
| $x_{ij}^f$                | Binary variable: 1 if vehicle $f \in F$ traverses edge $(i, j) \in E$ , 0 otherwise              |
| $z_u$                     | Binary variable: 1 if rider $u \in U$ is served (all requests in $R_u$ fulfilled), 0 otherwise   |
| $T_i^f$                   | Continuous variable: arrival time of vehicle $f \in F$ at node $i \in N$                         |
| $Q_i^f$                   | Continuous variable: load in vehicle $f \in F$ upon departure at node $i \in N$                  |
| $y_r$                     | Binary variable: 1 if trip request $r \in R$ is served, 0 otherwise                              |
| $\lambda_\theta$          | Binary variable: 1 if route $\theta \in \Omega$ is selected, 0 otherwise                         |

## 2.2 An Arc-Based Model

Figure 1 presents an arc-based model for the JRTPCSSP. The model is defined on the graph  $g = (N, E)$ , where  $N$  denotes the set of nodes and  $E$  the set of edges. Each trip request  $r \in R$  is represented by a pickup node  $i$  and a corresponding drop-off node  $n + i$ , included in the pickup node set  $P$  and the drop-off node set  $D$ , respectively, where  $n = |R|$ . Additionally, an origin depot node 0 and a destination depot node  $2n + 1$  are created for the physical depot, leading to the definition  $N = \{0\} \cup P \cup D \cup \{2n + 1\}$ . The set  $E$  comprises edges that connect nodes in  $N$ , with all connections subject to time window constraints. Each node  $i \in N$  is associated with a demand  $d_i$ , a service time  $s_i$ , and a time window  $[a_i, b_i]$  that corresponds to the earliest and latest service start time at node  $i$ . Note that  $a_0 = a_{2n+1}$  and  $b_0 = b_{2n+1}$  represent the earliest shift start time  $\xi_s$  and the latest shift end time  $\xi_e$ , respectively. For each edge  $(i, j) \in E$ , the travel time between nodes  $i$  and  $j$  is denoted by  $t_{ij}$ .

$$\max \sum_{f \in F} \sum_{i \in P} x^f(\delta^+(i)) \quad (1a)$$

$$\text{s.t.} \quad \sum_{f \in F} x^f(\delta^+(i)) = z_u \quad \forall u \in U, \forall i \in P_u, \quad (1b)$$

$$x^f(\delta^+(i)) - x^f(\delta^+(n + i)) = 0 \quad \forall i \in P, \forall f \in F, \quad (1c)$$

$$x^f(\delta^+(i)) - x^f(\delta^-(i)) = \begin{cases} 1 & \text{if } i = 0 \\ -1 & \text{if } i = 2n + 1 \\ 0 & \text{if } i \in P \cup D \end{cases} \quad \forall i \in N, \forall f \in F, \quad (1d)$$

$$(T_i^f + s_i + t_{ij})x_{ij}^f \leq T_j^f \quad \forall (i, j) \in E, \forall f \in F, \quad (1e)$$

$$a_i \leq T_i^f \leq b_i \quad \forall i \in N, \forall f \in F, \quad (1f)$$

$$T_{2n+1}^f - T_0^f \leq \eta \quad \forall f \in F, \quad (1g)$$

$$(Q_i^f + d_j)x_{ij}^f \leq Q_j^f \quad \forall (i, j) \in E, \forall f \in F, \quad (1h)$$

$$\max(0, d_i) \leq Q_i^f \leq \min(C, C + d_i) \quad \forall i \in N, \forall f \in F, \quad (1i)$$

$$x_{ij}^f \in \{0, 1\} \quad \forall (i, j) \in E, \forall f \in F, \quad (1j)$$

$$z_u \in \{0, 1\} \quad \forall u \in U \quad (1k)$$

Figure 1: The Arc-Based Model.

The binary decision variable  $x_{ij}^f$  determines whether vehicle  $f \in F$  traverses edge  $(i, j)$ . For simplicity, let  $x^f(\delta^+(i)) = \sum_{(i,j) \in \delta^+(i)} x_{i,j}^f$  and  $x^f(\delta^-(i)) = \sum_{(j,i) \in \delta^-(i)} x_{j,i}^f$  denote the sum of outgoing and incoming flows to node  $i$ , respectively, where  $\delta^+(i)$  and  $\delta^-(i)$  represent the sets of outgoing and incoming edges of node  $i \in N$ .

The objective function, defined in equation (1a), aims at maximizing the number of trip requests served. Constraint (1b) enforces the complete service requirement for each rider  $u \in U$ . The binary variable  $z_u$  indicates whether rider  $u$  is served ( $z_u = 1$ ) or not ( $z_u = 0$ ). The constraint links this variable to the service status of all pickup nodes  $i$  belonging to the set  $P_u$  (the set of pickup nodes associated with rider  $u$ 's requests  $R_u$ ). By requiring  $\sum_{f \in F} x^f(\delta^+(i))$  to equal the same value  $z_u$  for all  $i \in P_u$ , this constraint ensures that if any one of rider  $u$ 's requests is served, all of their other requests must also be served by some vehicle in the fleet  $F$ . Constraint (1c) enforces that pickup and drop-off services for each trip request are completed by the same vehicle. Constraint (1d) ensures flow balance, and constraint (1e) updates the variables  $T_i^f$ , arrival

time of vehicle  $f$  at node  $i$ . Constraint (1f) enforces time window requirements at node  $i$ . Constraint (1g) specifies the maximum working hours of each driver. Constraint (1h) updates the variables  $Q_j^f$ , the number of riders in vehicle  $f$  after visiting node  $j$ . Constraint (1i) specifies the bounds of  $Q_i^f$ . Lastly, constraints (1j) and (1k) define the domains of the decision variables.

Solutions from the arc-based model (1) provide insights for both rider trip planning and crew shift scheduling. On the rider side, the solutions indicate whether a rider can be served, and if so, by which vehicle and at what time. On the driver side, the solutions guide which riders to serve and when. In addition,  $T_0^f$  and  $T_{2n+1}^f$  represent the departure and arrival times at the depot, which can be used to determine crew shifts. While the model formulation in Figure 1 is nonlinear, it can be easily linearized since the variables  $x_{ij}^f$  are binary.

### 2.3 A Path-Based Model

Off-the-shell solvers such as Gurobi or CPLEX are not capable of directly solving large-scale instances encountered in practice when using the arc-based formulation presented in Section 2.2. Instead, AGGNNI-CG adopts a path-based model, presented in Figure 2, which corresponds to a Dantzig-Wolfe decomposition of the arc-based formulation. This reformulation is well-established in the vehicle routing literature and has demonstrated strong computational performance for the classical VRP and its variants (Cordeau, Jean-Francois and Groupe d'études et de recherche en analyse des décisions (Montréal, Québec), 2000; Toth and Vigo, 2014). On many practical applications, the path-based formulation can leverage column generation to find high-quality solutions more efficiently, as demonstrated in prior studies (e.g., Riley et al. (2019); Lu et al. (2022)).

$$\max \sum_{r \in R} y_r \quad (2a)$$

$$\text{s.t.} \quad y_r \leq \sum_{\theta \in \Omega} \alpha_{r\theta} \lambda_\theta \quad \forall r \in R, \quad (2b)$$

$$y_r = y_{r'} \quad \forall u \in U, \forall r, r' \in R_u, \quad (2c)$$

$$\sum_{\theta \in \Omega} \lambda_\theta \leq |F| \quad , \quad (2d)$$

$$\lambda_\theta \in \{0, 1\} \quad \forall \theta \in \Omega, \quad (2e)$$

$$y_r \in \{0, 1\} \quad \forall r \in R \quad (2f)$$

Figure 2: The Path-Based Model.

The objective function, defined in equation (2a), aims at maximizing the number of fulfilled trip requests. The binary variable  $y_r$  indicates whether a trip request  $r$  is served. The right-hand side of constraint (2b) denotes whether request  $r$  is served by the selected routes from the set  $\Omega$ . Here,  $\alpha_{r\theta}$  represents whether request  $r$  is served by route  $\theta \in \Omega$ , and the binary variable  $\lambda_\theta$  indicates whether route  $\theta$  is selected. Constraint (2c) ensures complete servicing of each rider requests without partial fulfillment. Constraint (2d) controls the maximum number of vehicles that can be deployed. Lastly, constraints (2e) and (2f) define the domains for the decision variables  $\lambda_\theta$  and  $y_r$ , respectively.

Each  $\theta \in \Omega$  is a feasible vehicle route that satisfies constraints (1c) to (1k). Therefore, each vehicle route  $\theta$  not only contains trip service schedules but also provides driver shift information. The major challenge

of solving Model (2) is to find feasible routes and construct the route set  $\Omega$ . The size of set  $\Omega$  increases exponentially with the number of trip requests. Hence, it is practically impossible to enumerate all routes in the set. Section 3 demonstrates how column generation is used to iteratively add promising routes to the set  $\Omega$ , avoiding the need to enumerate all possible routes.

### 3 The Column Generation Algorithm

This section introduces the column generation algorithm for solving the JRTPCSSP. Starting with a customized decomposition strategy, we illustrate three major components of the column generation in this study, including the master problem, the pricing subproblem, and how to find feasible integer solutions. Readers are referred to Appendix A for more details.

#### 3.1 Problem Decomposition Based on Driver Shifts

As previously discussed, this goal of the JRTPCSSP is not only to design optimal trip service schedules but also to determine the driver shifts that best accommodate the time-varying travel demands from the riders. In practical operations, driver shifts typically commence at specific times (hourly or half-hourly) for management convenience. This observation underpins the initial step of column generation: *the generation of the candidate set for driver shifts*. It is important to emphasize that, in the solution, multiple drivers can use the same shifts and some shifts may not be used at all. It is the role of column generation to determine the best driver shifts to serve as many requests as possible.

For concreteness, consider a scenario with the earliest shift start time  $\xi_s$  and latest shift end time  $\xi_e$ , and a maximum driver working duration of  $\eta$  hours. Assuming a time interval  $\delta$  between adjacent shift candidates, the candidate set  $\Phi$  for driver shifts can be defined as

$$\Phi = \{\phi = (dr_s, dr_e) \mid dr_s = \xi_s + k\delta, dr_e = dr_s + \eta, 0 \leq k \leq \lceil \frac{(\xi_e - \xi_s - \eta)}{\delta} \rceil, k \in \mathbb{Z}\}, \quad (3)$$

where each element  $\phi = (dr_s, dr_e) \in \Phi$  represents a driver shift, with  $dr_s$  and  $dr_e$  indicating its start and end times, respectively. Figure 3 illustrates such a candidate set for  $\xi_s = 5$ ,  $\xi_e = 22$ ,  $\eta = 8$ , and  $\delta = 1$ .

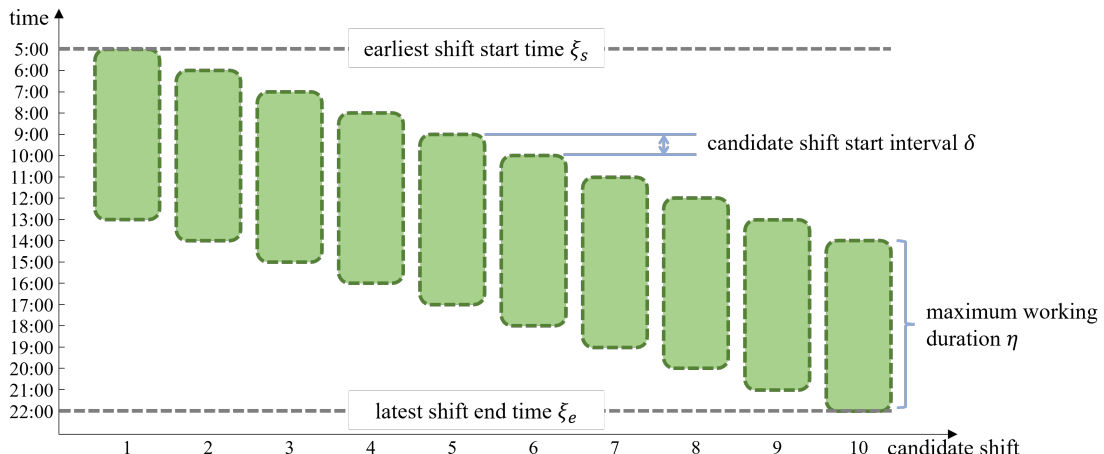


Figure 3: A Potential Candidate Set for Driver Shifts on a Particular Day.

The Restricted Linear Master Problem (RLMP) of the column generation algorithm is presented in Figure 4. The model uses a given candidate set  $\Phi$  of driver shifts and relaxes the integrality of the decision variables  $\lambda_\theta$  and  $y_r$ . Additionally, a restricted route set  $\Omega'_\phi$  is introduced for each driver shift candidate  $\phi \in \Phi$ : it contains a subset of feasible vehicle routes corresponding to driver shift  $\phi$ .

$$\max \sum_{r \in R} y_r \quad (4a)$$

$$\text{s.t.} \quad y_r \leq \sum_{\phi \in \Phi} \sum_{\theta \in \Omega'_\phi} \alpha_{r\theta} \lambda_\theta \quad \forall r \in R, \quad (4b)$$

$$y_r = y_{r'} \quad \forall u \in U, \forall r, r' \in R_u, \quad (4c)$$

$$\sum_{\phi \in \Phi} \sum_{\theta \in \Omega'_\phi} \lambda_\theta \leq |F| \quad , \quad (4d)$$

$$\lambda_\theta \in [0, 1] \quad \forall \theta \in \bigcup_{\phi \in \Phi} \Omega'_\phi, \quad (4e)$$

$$y_r \in [0, 1] \quad \forall r \in R \quad (4f)$$

Figure 4: The Restricted Linear Master Problem.

For each  $\Omega'_\phi$ , promising feasible routes using driver shift  $\phi$  are iteratively added by solving pricing subproblems. Pricing subproblems corresponding to different driver shifts are completely independent. Therefore, in the pricing stage, the original pricing subproblem can be decomposed to  $|\Phi|$  independent pricing problems that can be solved in parallel.

It is important to note that a finer granularity in the driver shift set  $\Phi$ , determined by  $\delta$ , does not substantially increase the complexity of identifying promising routes in these subproblems. This is because each subproblem is independent and can be processed in parallel. Furthermore, a higher number of subproblems potentially introduces more promising routes in each column generation iteration, which may reduce the total number of iterations required.

### 3.2 The Pricing Subproblem

Each column generation iteration adds, for each driver shift  $\phi \in \Phi$ , new promising routes in  $\Omega'_\phi$  by solving the pricing subproblem shown in Figure 5. In the objective function (5a),  $\pi_r$  and  $\sigma$  denote the dual values of constraints (4b) and (4d) after solving Problem (4). The pricing subproblem seeks a feasible vehicle route that minimizes the reduced cost. This problem can be modeled as a shortest path problem with resource constraints, a common approach in column generation for vehicle routing problems (Feng et al., 2024). The goal is to find a path from the starting depot to the ending depot in the graph  $g = (N, E)$  such that the path's total reduced cost is minimized, while adhering to the resource constraints in (1c) - (1k).

In AGGNNI-CG, this pricing subproblem is solved using dynamic programming. The specifics of this dynamic programming approach, including the label definition and extension process, are detailed in Algorithm 3 in Appendix A. The dynamic programming implementation does not solve the pricing subproblem to optimality for each driver shift, which can be very time-consuming. Instead, the dynamic programming process stops as soon as a fixed number of routes with negative reduced costs has been generated. Note that the early stop strategy does not affect the optimality of the algorithm.

$$\begin{aligned}
\min \quad & - \sum_{r \in R} \pi_r y_r - \sigma \\
\text{s.t.} \quad & (1c) - (1k)
\end{aligned} \tag{5a}$$

Figure 5: The Pricing Subproblem For Driver Shift  $\phi$ .

Preliminary experiments indicated that, for large-scale instances, even with the early stop strategy, it remains challenging to generate a sufficient number of promising routes with negative costs within an acceptable timeframe. To address this, the column generation implements two heuristics. First, in the dynamic programming process, at each node  $i \in N$ , only a limited number of labels with the lowest reduced costs are retained. Second, during column generation, if the value of the objective function (4a) remains unchanged for a specified number of iterations, the process is terminated early. It is important to note that these heuristics, along with the one mentioned in the next subsection, may affect the ability of the column generation algorithm in finding an optimal solution.

### 3.3 Finding Feasible Integer Solutions

The column generation often produces solutions that are fractional, rendering them infeasible for the original model detailed in formulation (2). To obtain integer solutions, the column generation algorithm is typically embedded within a branch-and-bound framework. Two primary approaches are prevalent for branching strategies: edge-based and path-based. Edge-based branching tends to yield more balanced subproblems, whereas path-based branching is more efficient in rapidly identifying integer feasible solutions.

However, preliminary experiments revealed that, given the high complexity and large scale of the problems in this study, neither exact edge-based nor path-based branching strategies could produce feasible solutions within a reasonable time frame. Consequently, the column generation developed in this study employs a path-based branching strategy complemented by a straightforward heuristic. Specifically, if the optimal solution of the RMLP is fractional, the variable associated with the column with the largest fractional  $\lambda_\theta$  value is fixed to 1 and a new phase of the column generation algorithm is initiated. This process is repeated until an integer feasible solution is obtained.

## 4 Boosting Column Generation with Machine Learning

In the column generation method outlined in Section 3, the most computationally intensive components are the pricing subproblems, which are NP-hard as they involve finding the shortest paths with resource constraints. To overcome this computational challenge, AGGNNI-CG leverages machine learning to speed up pricing subproblems. This section presents AGGNNI-CG (Attention and Gated GNN-Informed Column Generation), a framework that leverages machine learning to speed up and improve the quality of column generation for real-life applications where trip demands exhibit stable patterns over time. The framework extract insights from historical data to inform and guide the solution of new problem instances.

## 4.1 The Machine Learning Framework

The AGGNNI-CG framework is depicted in Figure 6. Its key strategy is to reduce the number of edges to explore in the pricing subproblems. In other words, before applying column generation, AGGNNI-CG simplifies the graph of a new instance by discarding edges unlikely to yield high-quality routes.

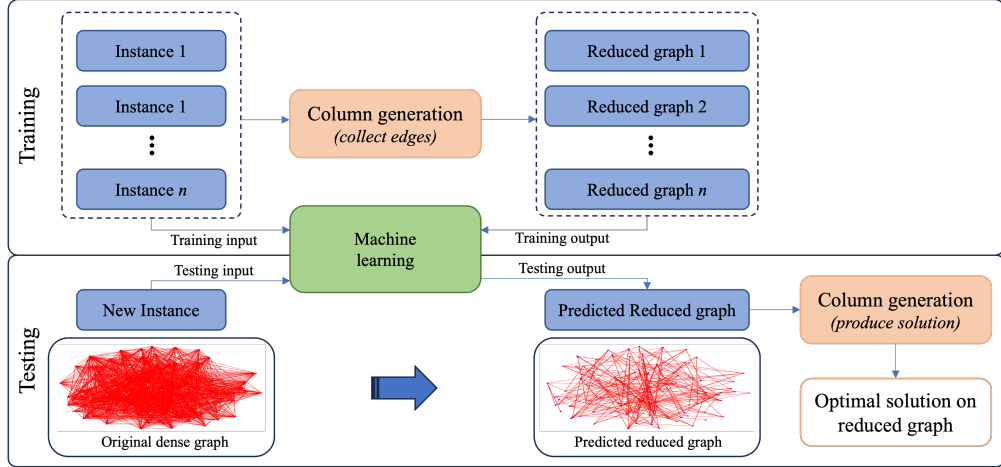


Figure 6: The Machine Learning Framework of AGGNNI-CG.

To determine which edges belong to high-quality or optimal routes, AGGNNI-CG uses routes generated in the pricing subproblems of historical instances. The training of machine learning model of AGGNNI-CG uses a dataset of historical instances and their solutions using the the column generation algorithm introduced in Section 3. Edges that frequently appear across column generation iterations are earmarked as *promising*. These promising edges make it possible to define reduced graph for each historical instance. The historical reduced graphs are key input to the machine learning, as shown in the top part of Figure 6.

AGGNNI-CG then trains a machine learning model in a supervised manner: the training optimization receives as inputs the historical graphs of each instance and the reduced graphs. In real time, AGGNNI-CG applies the machine learning to a new instance and obtains its reduced graph. The column generation algorithm is applied to the reduced instance. The reduced graph, with fewer edges, allows the pricing subproblems to be solved more quickly, greatly improving the overall efficiency of the column generation process. In practice, the instances come with different nodes and different edges. As a result, AGGNNI-CG uses a Graph Neural Network (GNN) (Kipf and Welling, 2016) for the learning task. For each instance, the inputs for training the GNN model are the graph structure and encodings of the nodes and edges (see Section 4.3). The GNN architecture predicts which edges are promising for any instance represented in this way. Additionally, Section 4.6 explores how to classify an edge as promising in the training data.

## 4.2 Overview of The GNN-Based Architecture

The GNN architecture of AGGNNI-CG is illustrated in Figure 7. Table 2 provides a complete glossary of terms used in the GNN model, including inputs, outputs, learnable parameters, auxiliary variables, and loss function parameters. The GNN model is presented mathematically in Figure 8, and the training optimization problem is shown in Figure 9. The rest of this section introduces each concept incrementally.

As mentioned earlier, the GNN receives, as input, a graph structure, the node encodings, and the edge encodings. The GNN then applies several graph convolutional layers, starting with a graph attention layer

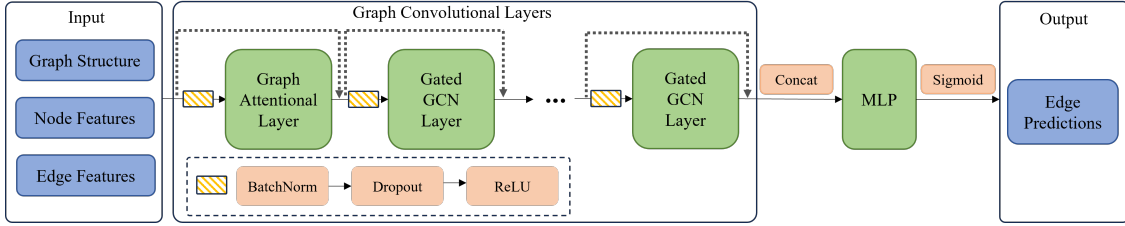


Figure 7: The GNN Architecture of AGGNNI-CG.

Table 2: Glossary: Inputs, Outputs, Learnable Parameters, and Loss Function Parameters.

| Inputs:                   | $g = (N^g, E^g)$  | the graph   |
|---------------------------|---|---|
| $\mathbf{h}_i^g$          | the initial embedding of node $i$ in $g$  |   |
| $\mathbf{e}_{ij}^g$       | the initial embedding of edge $(i, j)$ in $g$   |   |
| $p_{ij}^g$                | the label for edge $(i, j)$ of $g$  |   |
| Outputs:                  | $\hat{p}_{ij}^g$  | the prediction for edge $(i, j)$ of $g$   |
| Learnable Parameters:     | $\mathbf{W}_{1,h}, \mathbf{W}_{2,h}, \mathbf{W}_{3,h}, \mathbf{a}_h$<br>$\mathbf{W}_{4,h}, \mathbf{W}_{5,h}$<br>$\Theta_{1,\ell}, \Theta_{2,\ell}, \Theta_{3,\ell}, \Theta_{4,\ell}$<br>$\text{MLP}$<br>$\Pi$ | edge attention (head $h$ )<br>node attention (head $h$ )<br>residual gated graph (layer $\ell$ )<br>decoder as a multi-layer perceptron<br>the collection of all learnable parameters |
| Auxiliary Values:         | $\mathbf{h}_i^{g,\ell}$<br>$\gamma_{ij}^{g,h}$<br>$\kappa_{ij}^{g,\ell}$  | transformed embedding for node $i$ in layer $\ell$ in $g$<br>attention of edge $(i, j)$ for head $h$ in $g$<br>gate of edge $(i, j)$ for layer $\ell$ in $g$                          |
| Loss Function Parameters: | $w^1, w^0$<br>$\alpha_L$  | label class weights<br>L1-Norm penalty  |

before a series of gated graph convolutional layers. These layers transform the node encodings. The graph convolutional layers are followed by a multi-layer perceptron that takes, as inputs, the transformed encodings of every edge in the graph and produces an output that is then run through a sigmoid function to estimate the likelihood of an edge to be promising. More formally, the GNN architecture defines a parametric function

$$\mathcal{M}_{\Pi}((N^g, E^g), \{\mathbf{h}_i^g\}_{i \in N^g}, \{\mathbf{e}_{ij}^g\}_{(i,j) \in E^g})$$

which receives, as inputs, a graph structure  $(N^g, E^g)$ , a node encoding  $\{\mathbf{h}_i^g\}_{i \in N^g}$ , and an edge encoding  $\{\mathbf{e}_{ij}^g\}_{(i,j) \in E^g}$ . It returns the likelihood  $\hat{p}_{ij}^g$  that an edge be promising for the column generation for each edge  $(i, j) \in E^g$ . The function is parametrized by a set of learnable parameters  $\Pi$ .

The GNN architecture uses the graph structure as an input, so that it can be applied to graphs of different sizes and shapes. Moreover, node and edge encodings make it possible to apply the architecture for instances

---


$$\mathcal{M}_{\Pi}((N^g, E^g), \{\mathbf{h}_i^g\}_{i \in N^g}, \{\mathbf{e}_{ij}^g\}_{(i,j) \in E^g}) :$$

$$\begin{aligned} \gamma_{ij}^{g,h} &= \frac{\exp(\mathbf{a}_h^\top \text{LeakyReLU}(\mathbf{W}_{1,h} \mathbf{h}_i^g + \mathbf{W}_{2,h} \mathbf{h}_j^g + \mathbf{W}_{3,h} \mathbf{e}_{ij}^g))}{\sum_{k \in N(i) \cup \{i\}} \exp(\mathbf{a}_h^\top \text{LeakyReLU}(\mathbf{W}_{1,h} \mathbf{h}_i^g + \mathbf{W}_{2,h} \mathbf{h}_k^g + \mathbf{W}_{3,h} \mathbf{e}_{ik}^g))} & (i,j) \in E^g, h \in H \\ \mathbf{h}_i^{g,1} &= \sum_{h=1}^H \gamma_{ii}^{g,h} \mathbf{W}_{4,h} \mathbf{h}_i^g + \sum_{j \in N(i)} \gamma_{ij}^{g,h} \mathbf{W}_{5,h} \mathbf{h}_j^g & i \in N^g \\ \kappa_{ij}^{g,\ell} &= \sigma(\Theta_{3,\ell} \mathbf{h}_i^{g,\ell-1} + \Theta_{4,\ell} \mathbf{h}_j^{g,\ell-1}) & (i,j) \in E^g, \ell \in 2 \dots L \\ \mathbf{h}_i^{g,\ell} &= \Theta_{1,\ell} \mathbf{h}_i^{g,\ell-1} + \sum_{j \in N(i)} \kappa_{ij}^{g,\ell} \odot \Theta_{2,\ell} \mathbf{h}_j^{g,\ell-1} & i \in N^g, \ell \in 2 \dots L \\ \hat{p}_{ij}^g &= \sigma(\text{MLP}(\{\mathbf{h}_i^{g,L} \parallel \mathbf{h}_j^{g,L}\})) & (i,j) \in E^g \\ \text{return} &\{\hat{p}_{ij}^g\}_{(i,j) \in E^g} \end{aligned}$$


---

Figure 8: The Machine Learning GNN Model for Predicting Promising Edges.

$$\begin{aligned} \min_{\Pi} \quad & \sum_{m=1}^M \sum_{(i,j) \in E^{g_m}} (w^1 p_{ij}^{g_m} \log(\hat{p}_{ij}^{g_m}) + w^0 (1 - p_{ij}^{g_m}) \log(1 - \hat{p}_{ij}^{g_m})) + \alpha_L \sum_{(i,j) \in E^{g_m}} \hat{p}_{ij}^{g_m} \\ \text{s.t.} \quad & \{\hat{p}_{ij}^{g_m}\}_{(i,j) \in E^{g_m}} = \mathcal{M}_{\Pi}((N^{g_m}, E^{g_m}), \{\mathbf{h}_i^{g_m}\}_{i \in N^{g_m}}, \{\mathbf{e}_{ij}^{g_m}\}_{(i,j) \in E^{g_m}}) \quad \forall m \in M \end{aligned}$$


---

Figure 9: The Optimization Model for Training the GNN Model.

with nodes and edges that have not been seen before. The GNN architecture transforms a node encoding through multiple layers, using its encoding and the encodings of its neighbors. The learnable parameters do not depend on the specific graph structure of each instance: they are *shared* by all instances and only apply to the node and edge embeddings. GNNs are especially attractive in the setting of this paper, since JRTPCSSP instances may have different sets of nodes and different sets of edges. Indeed, the number of requests can fluctuate significantly from day to day, resulting in graphs of different sizes.

### 4.3 Feature Encoding

For each graph instance  $(N^g, E^g)$ , AGGNNI-CG extracts features to characterize each node  $i \in N^g$ . Specifically, the feature vector  $\mathbf{h}_i^g$  for node  $i$  include its geographic coordinates (latitude and longitude), its time window, and a categorical indicator showing whether the node is a pickup, drop-off, or depot. In addition, AGGNNI-CG considers features for each edge  $(i,j) \in E^g$ . The edge feature vector  $\mathbf{e}_{ij}^g$  includes the travel time from node  $i$  to node  $j$  and a binary indicator of whether  $(i,j)$  directly connects the origin and destination of the same trip. To ensure consistency across different input instances, AGGNNI-CG applies a min-max scaler to normalize each feature to the range  $[0, 1]$ . This feature selection aligns with standard practices in the literature, following similar approaches in machine learning applications for routing problems (Joshi et al., 2019; Yuan et al., 2022b; Morabit et al., 2023). Appendix B provides a detailed analysis of the relative importance of the proposed features.

## 4.4 The GNN Architecture

The section details the GNN architecture for an input  $((N^g, E^g), \{\mathbf{h}_i^g\}_{i \in N^g}, \{\mathbf{e}_{ij}^g\}_{(i,j) \in E^g})$ .

### 4.4.1 The Graph Convolutional Layers

The node embeddings are first updated through one layer of the multi-head graph attentional operator (GATConv), the core of the Graph Attention Network (GAT) architecture from (Veličković et al., 2017; Brody et al., 2021). In contrast to classical graph convolutional networks which employ equal-weight neighborhood aggregation, the multi-head attention mechanism allows for the assignment of different weights to different neighbor nodes. Taking the edge encodings into consideration, AGGNNI-CG computes the attention weight  $\gamma_{ij}^{g,h}$  between a pair of nodes  $i$  and  $j$  for a head  $h$  as follows:

$$\gamma_{ij}^{g,h} = \frac{\exp(\mathbf{a}_h^\top \text{LeakyReLU}(\mathbf{W}_{1,h} \mathbf{h}_i^g + \mathbf{W}_{2,h} \mathbf{h}_j^g + \mathbf{W}_{3,h} \mathbf{e}_{ij}^g))}{\sum_{k \in N(i) \cup \{i\}} \exp(\mathbf{a}_h^\top \text{LeakyReLU}(\mathbf{W}_{1,h} \mathbf{h}_i^g + \mathbf{W}_{2,h} \mathbf{h}_k^g + \mathbf{W}_{3,h} \mathbf{e}_{ik}^g))} \quad (7)$$

$$\text{LeakyReLU}(x) = \begin{cases} x & \text{if } x > 0, \\ 0.2x & \text{if } x \leq 0. \end{cases}, \quad (8)$$

where  $N(i)$  corresponds to the neighbors of node  $i$ , while  $\mathbf{a}$ ,  $\mathbf{W}_1$ ,  $\mathbf{W}_2$ , and  $\mathbf{W}_3$  are learnable parameters. Intuitively,  $\gamma_{ij}$  measures the significance of node  $j$  for node  $i$ .

After obtaining the attention weights for each edge, AGGNNI-CG updates the node embeddings of each node  $i$  by calculating the weighted sum of the transformed features of its neighbors and itself, i.e.,

$$\gamma_{ii}^{g,h} \mathbf{W}_{4,h} \mathbf{h}_i^g + \sum_{j \in N(i)} \gamma_{ij}^{g,h} \mathbf{W}_{5,h} \mathbf{h}_j^g \quad (9)$$

Since the implementation uses a multi-head attention with  $H > 1$  attention heads, the node embeddings are updated by concatenating  $H$  independent attention mechanisms following Equation (9):

$$\mathbf{h}_i^{g,1} = \parallel_{h=1}^H \gamma_{ii}^{g,h} \mathbf{W}_{4,h} \mathbf{h}_i^g + \sum_{j \in N(i)} \gamma_{ij}^{g,h} \mathbf{W}_{5,h} \mathbf{h}_j^g \quad (10)$$

where  $\parallel$  denotes the concatenation operator, while  $\gamma_{ij}^{g,h}$  represents the attention weights for the  $h$ -th attention mechanism and edge  $(i, j)$ . The matrices  $\mathbf{W}_{4,h}$  and  $\mathbf{W}_{5,h}$  are the corresponding learnable parameters. Figures 10 and 11 provide visualizations of the process occurring within the graph attentional layer.

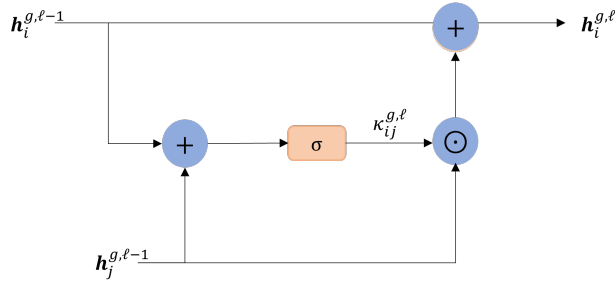
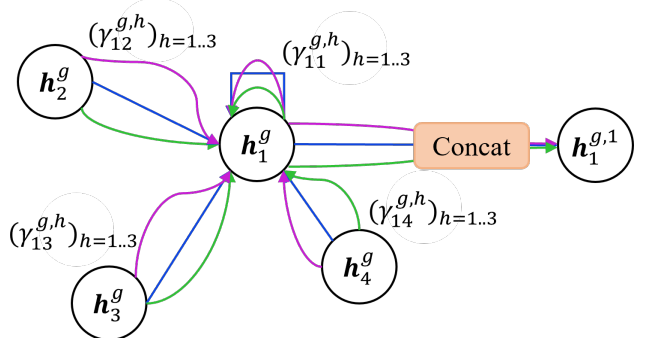
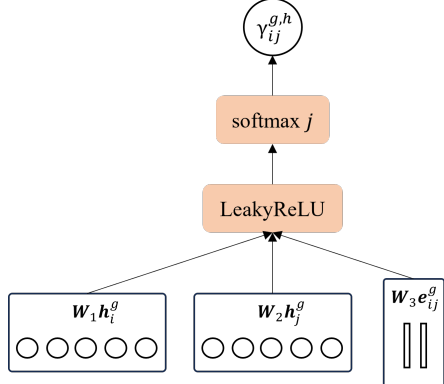
Subsequently, the node embeddings are fed into multiple layers of the Residual Gated Graph ConvNets (GCN), which has been used in several related studies (Joshi et al., 2019; Yuan et al., 2022b). The number of Residual Gated GCN layers is considered as a hyperparameter, which is fine-tuned during the experiments. For each layer  $2 \leq \ell \leq L$ , the node embeddings are updated following a gating mechanism described in (Bresson and Laurent, 2017):

$$\mathbf{h}_i^{g,\ell} = \Theta_{1,\ell} \mathbf{h}_i^{g,\ell-1} + \sum_{j \in N(i)} \kappa_{ij}^{g,\ell} \odot \Theta_{2,\ell} \mathbf{h}_j^{g,\ell-1} \quad (11)$$

with the gate  $\kappa_{ij}^{g,\ell}$  defined as:

$$\kappa_{ij}^{g,\ell} = \sigma(\Theta_{3,\ell} \mathbf{h}_i^{g,\ell-1} + \Theta_{4,\ell} \mathbf{h}_j^{g,\ell-1}) \quad (12)$$

where  $\odot$  denotes the element-wise multiplication operator. The matrices  $\Theta_{1,\ell}, \Theta_{2,\ell}, \Theta_{3,\ell}, \Theta_{4,\ell}$  are learnable parameters for the  $\ell$ -th gated GCN layer, and  $\sigma(\cdot)$  represents the Sigmoid function. The gating mechanism is illustrated in Figure 12.



The model performance was enhanced by applying established methods to the node embeddings before they enter each graph convolutional layer. Batch normalization and dropouts stabilize training and prevent overfitting. Moreover, the GNN also incorporates skip (residual) connections to amplify the influence of the embeddings generated in the initial layers. This approach has shown empirical success in improving node differentiation within the model.

#### 4.4.2 The Decoder

After the graph convolutional layers generate the final node embeddings, AGGNNI-CG converts them into edge embeddings by concatenating the embeddings of the two nodes that form each edge. The concatenated embeddings are then passed through a multi-layer perceptron (MLP) consisting of fully connected layers followed by ReLU activations. Finally, a Sigmoid function is applied to the MLP outputs to ensure they fall within  $[0, 1]$ . The result is an estimated probability score  $\hat{p}_{ij}^g$  for each edge, representing the likelihood that edge  $(i, j)$  belongs to the set of promising edges. The process is captured via the following equation:

$$\hat{p}_{ij}^g = \sigma \left( \text{MLP} \left( \{ \mathbf{h}_i^{g,L} \| \mathbf{h}_j^{g,L} \} \right) \right). \quad (13)$$

## 4.5 The Training Loss Function

The training optimization is depicted in Figure 9. It receives, as input, a collection of  $M$  instances with the associated labels for each edge. The training optimization uses the GNN presented earlier to predict the likelihood of an edge to be promising. The training uses binary cross-entropy as its loss function during training, which is a standard choice for most binary classification tasks, and minimizes empirical risk, i.e.,

$$\sum_{m=1}^M \sum_{(i,j) \in E^{g_m}} (w^1 p_{ij}^{g_m} \log(\hat{p}_{ij}^{g_m}) + w^0 (1 - p_{ij}^{g_m}) \log(1 - \hat{p}_{ij}^{g_m})),$$

where instance  $m$  is specified by  $((N^{g_m}, E^{g_m}), \{\mathbf{h}_i^{g_m}\}_{i \in N^{g_m}}, \{\mathbf{e}_{ij}^{g_m}\}_{(i,j) \in E^{g_m}})$  and the labels  $\{p_{ij}^{g_m}\}_{(i,j) \in E^{g_m}}$ . To further enhance the model performance, AGGNNI-CG incorporates an L1 regularization term in the loss function

$$\alpha_L \sum_{(i,j) \in E^{g_m}} \hat{p}_{ij}^{g_m},$$

encouraging sparsity in the model's output probabilities.

## 4.6 Labeling Historical Data

It remains to specify how to label historical data for training the machine learning architecture. Indeed, the effectiveness of machine learning model training hinges on the criteria for selecting edges to construct the reduced graph for each training instance. In general, it is not sufficient to select edges from the paths chosen in the optimal solutions. These sets may not allow the subsequent column generation procedure to find feasible solutions to unseen instances or find solutions of high quality. Moreover, the complexity of JRPCSSP led to a number of heuristic decisions in the column generation procedure that may negatively impact the learning process. For these reasons, the promising edges used in the labeling process of AGGNNI-CG come from five classes:

1. RGTrn-A: these are the edges from all paths explored during column generation iterations, i.e., paths in  $\bigcup_{\phi \in \Phi} \Omega'_\phi$ .
2. RGTrn-U: these are the edges selected in a solution (path) of the RLMP, i.e., they have a non-zero value in an RLMP.
3. RGTrn-U $x$ : The top  $x \in \{80, 50, 30\}$  percent of edges in RGTrn-U, ranked by number of times they were used in all RLMP solutions.

Note that the label is 1 for a promising edge (i.e., an edge in the selected set); it is zero otherwise.

## 4.7 Using Reduced Graph in Column Generation

During inference, the GNN model described in Figure 8 generates probability estimates  $\hat{p}_{ij}^g \in [0, 1]$  for each edge  $(i, j)$  in an unseen instance graph  $g = (N^g, E^g)$ . These estimates represent the likelihood that an edge belongs in the reduced graph used for column generation pricing subproblems. However, to create a practical reduced graph, these continuous probabilities must be converted to binary decisions (i.e., include or exclude the edge).

To systematically control the reduced graph's size, AGGNNI-CG employs a rank-based thresholding approach:

1. First, all edges in the original graph are ranked in descending order according to their predicted probability values  $\hat{p}_{ij}^g$ .
2. Only the top  $\tau$  percent of these sorted edges are retained for the reduced graph.
3. To ensure solution feasibility, certain critical edges are always preserved regardless of their predicted probabilities. Specifically, for each trip request  $r \in R$  with pickup node  $i$  and drop-off node  $n+i$ , the edges connecting the origin depot to pickup node, pickup node to drop-off node, and drop-off node to destination depot  $\{(0, i), (i, n+i), (n+i, 2n+1)\}$  are retained.

This thresholding process can be formally represented as an operator  $\mathcal{T}_\tau$  that takes the set of predicted probabilities and the original edge set as inputs, returning the reduced edge set  $E_{\text{reduced}-\tau}^g$ :

$$E_{\text{reduced}-\tau}^g = \mathcal{T}_\tau \left( \mathcal{M}_{\mathbf{H}} \left( (N^g, E^g), \{\mathbf{h}_i^g\}_{i \in N^g}, \{\mathbf{e}_{ij}^g\}_{(i,j) \in E^g} \right), E^g \right). \quad (14)$$

The resulting reduced graph  $g_{\text{reduced}-\tau} = (N^g, E_{\text{reduced}-\tau}^g)$  is then used in the column generation process. Specifically, in Algorithm 1, replace graph  $g = (N^g, E^g)$  with reduced graph  $g_{\text{reduced}-\tau} = (N^g, E_{\text{reduced}-\tau}^g)$  as an input.

The experiments in this paper explore the trade-off between computation time and solution quality by varying the threshold  $\tau$  between 2 and 30. For each value of  $\tau$ , the corresponding class of reduced test graphs is referred to as RGTst- $\tau$ .

## 5 Numerical Experiments

This section presents the experimental results. Section 5.1 describes the dataset, Section 5.2 presents the baselines, Section 5.3 reports the evaluation of the GNN, Section 5.4 compares AGGNNI-CG with the baselines under different configurations, and Section 5.5 describes the sensitivity analysis.

### 5.1 Dataset Description

AGGNNI-CG is evaluated using a real-world dataset derived from the Paratransit service in Chatham County, Georgia, U.S. This service caters to individuals with disabilities who are unable to use the regular public transportation system, offering them a reservation-based travel option. Riders are required to schedule their trips one day in advance, with the system ceasing to accept requests at 4 pm each day. At this cutoff time, the optimization of the driver shifts and trip schedules for the subsequent day begins. Due to constraints in the availability of drivers and vehicles, not all requests can be accommodated in general. The dataset encompasses information on daily trip requests spanning from January 2014 to December 2019. Each request includes the rider's origin, destination, and preferred pick-up and drop-off times.

As illustrated in Figure 13, the demand for trips is relatively stable year-over-year, an observation that is critical for the applicability of AGGNNI-CG. Figure 14 indicates that weekdays experience a higher demand for trips compared to weekends and holidays. To ensure consistency in the demand pattern, the experiments exclusively utilize weekday trip request data. The training of the graph neural network described in Section 4

is conducted using data from workdays between January 2014 and November 2019. Data from December 2019 serves as the basis for evaluating performance.

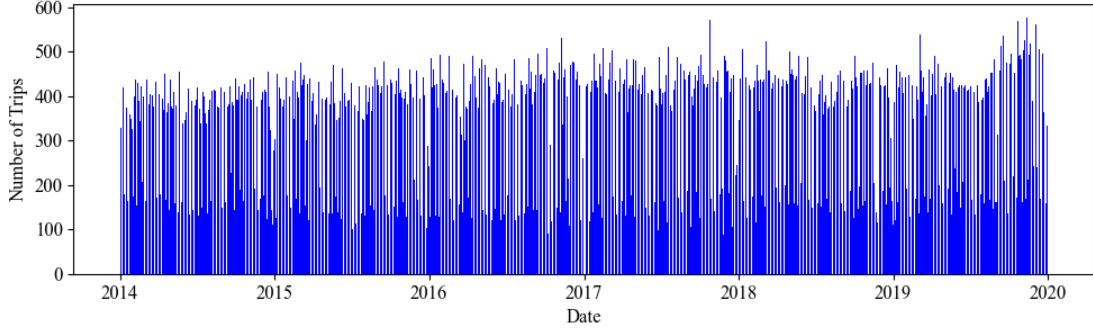


Figure 13: Daily Number of Trip Requests from January 2014 to December 2019.

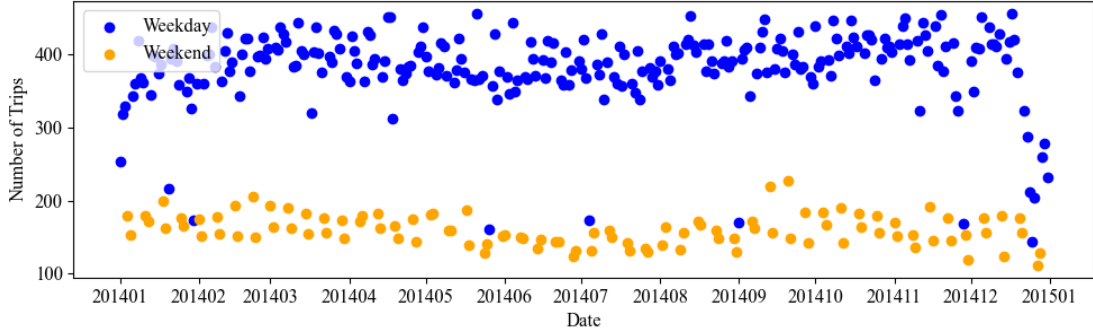


Figure 14: Daily Number of Trip Requests in 2014.

For the purposes of this study, the number of drivers allocated each day is determined by the volume of trip requests for that day, calculated as follows:

$$n_d = \left\lceil \frac{n_r}{\omega} \right\rceil, \quad (15)$$

where  $n_d$  denotes the number of drivers,  $n_r$  represents the number of trip requests, and  $\omega$  is the average number of trips a driver can manage in a day, which is set to 16 in this study.

## 5.2 Column Generation Approaches

The following three column generation approaches are compared in the evaluation.

1. Baseline-CG is the conventional column generation approach, which applies column generation described in Section 3 directly on original dense graphs without graph reduction.
2. RF-CG uses a Random Forest-based method for graph reduction, as outlined in [Morabit et al. \(2023\)](#). This approach has proven effective in a related Vehicle Routing Problem with Time Windows.
3. AGGNNI-CG is the proposed approach which leverages a GNN-based model for graph reduction.

By default, both RF-CG and AGGNNI-CG use the same configuration for graph reduction training and testing, i.e., RGTrn-U50 and RGTst-10, respectively.

### 5.3 Evaluation of the Graph Neural Network

This section evaluates the performance of the proposed GNN model on the real-world dataset described in Section 5.1. The model training was conducted on a single Nvidia Tensor Core H100 GPU on the PACE cluster ([Partnership for an Advanced Computing Environment \(PACE\), 2017](#)). The implementation of the graph convolutional layers was carried out using version 2.4.0 of the PyTorch Geometric library in Python 3.9. The loss function is minimized via gradient descent, using the Adam optimizer with weight decay as described in [Kingma and Ba \(2014\)](#). Each data point in the dataset corresponds to a single graph. For graph-level mini-batching, the training follows the method outlined in [PyTorch-Geometric \(2024\)](#), where adjacency matrices for the same mini-batch are stacked diagonally, and the node-level features are concatenated along the node dimension.

Given the disparity between class distributions, with the positive class accounting for merely 6% of the labels, the evaluation metrics are carefully selected to reflect a balanced view of the model’s performance. In line with [Morabit et al. \(2023\)](#), the results utilize Recall, Specificity, and Balanced Accuracy as primary metrics. *Recall*, i.e., the true positive rate, assesses the model effectiveness in accurately identifying all instances of the positive class. *Specificity*, i.e., the true negative rate, evaluates how precisely the model detects negatives in the majority class. As the aim is to maximize both these metrics, *Balanced Accuracy*, i.e., the average of Recall and Specificity, is also included to offer a comprehensive metric reflecting the model’s overall accuracy for both classes.

The dataset, excluding the test period, spans from January 2014 to November 2019 and includes a total of 1,539 instances. The dataset is partitioned in an 80-20 split for training and validation sets. An adaptive learning strategy is applied to optimize the training. If the validation loss showed no improvement over several epochs, indicating a learning plateau, the learning rate is lowered to nudge the model towards better performance. In cases where this adjustment did not lead to any further gains, and to prevent the model from overfitting, early stopping is initiated. This step was crucial to retain the model’s ability to generalize to new data. Additionally, the hyperparameters of the GNN model are tuned to maximize balanced accuracy on the validation set using Optuna ([Akiba et al., 2019](#)) with 100 trials. Table 3 presents the hyperparameter search space and the best configuration identified during the tuning process.

Table 3: GNN Hyperparameter Configuration: Search Space and Best Values Found

| Hyperparameter                     | Search Space                           | Best Value Found     |
|------------------------------------|--|----------------------|
| Dropout Rate                       | $\{0.30, 0.35, \dots, 0.70\}$          | 0.35                 |
| Hidden Dimensions                  | $\{64, 128, 256, 512\}$                | 256                  |
| L1 Regularization ( $\lambda_L$ )  | $[1 \times 10^{-8}, 1 \times 10^{-2}]$ | $4 \times 10^{-8}$   |
| Learning Rate                      | $[1 \times 10^{-5}, 1 \times 10^{-2}]$ | $4 \times 10^{-3}$   |
| Number of Attention Heads          | $\{4, 8, 16\}$                         | 8                    |
| Res-Gated GCN Layers               | $[2, 8]$                               | 6                    |
| Weight Decay                       | $[1 \times 10^{-8}, 1 \times 10^{-5}]$ | $6.8 \times 10^{-5}$ |
| Mini-batch Size                    | Fixed                                  | 4                    |
| Class Weight Ratio ( $w_+ : w_-$ ) | Fixed                                  | 15.65 : 1            |

The performance of the GNN model is compared to a Random Forest (RF) classification model described in [Morabit et al. \(2023\)](#). Unlike GNN, which leverages the entire graph structure, the RF model operates only at the edge level. RF learns the promising probability of each edge individually based on the features of the edge and its two endpoints. Since each training data point for RF is an edge, 30 days from the period

between January 2014 and November 2019 were sampled to keep the training set size manageable; all edges from each of these days are included. The features used for RF are aligned with those in the GNN model. In addition, the balanced class weights are adopted, and the hyperparameters are tuned similarly as in [Morabit et al. \(2023\)](#) to minimize the balanced accuracy.

The test set metrics, shown in Table 4, highlight the strong performance of the GNN model. With a recall of 90.2% (compared to 81.1% for RF), the GNN accurately identifies the majority of promising edges. Additionally, its specificity of 86.4% (compared to 77.8% for RF) demonstrates that the high recall does not come at the expense of incorrectly classifying negative instances. The balanced accuracy of 88.3% for the GNN is nearly 9% higher than for the RF model, further indicating that GNN is a more effective classifier overall. The results demonstrate that the GNN benefits from learning from the global graph topology, rather than relying solely on local connectivity information.

Table 4: Accuracy Metrics on the Test Set.

| Metric            | GNN (%) | RF (%) |
|-------------------|---------|--------|
| Recall            | 90.2    | 81.1   |
| Specificity       | 86.4    | 77.8   |
| Balanced Accuracy | 88.3    | 79.4   |

The Receiver Operating Characteristic (ROC) curve for GNN, shown in Figure 15, corroborates these findings. With an AUC of 0.95, the curve articulates the model’s substantial discriminative power, signifying a high true positive rate at various threshold levels while maintaining a low false positive rate. This high AUC is particularly telling of the model’s proficiency in distinguishing between the two classes. The ROC curve’s proximity to the upper left corner are indicative of an almost ideal classifier, striking an effective balance between sensitivity and specificity. This is particularly notable given the challenge of maintaining high sensitivity in this highly imbalanced dataset without compromising specificity.

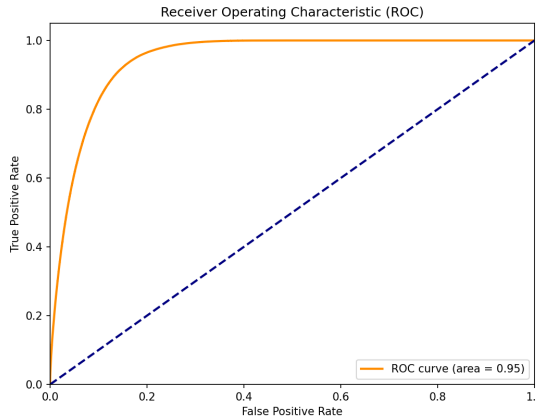


Figure 15: The ROC Curve for GNN Evaluated on the Test Set.

#### 5.4 Performance Analysis of the Column Generation

This section compares AGGNNI-CG with Baseline-CG and RF-CG. The analysis focuses on weekday data to account for the notable differences in trip request patterns between weekdays and weekends. Furthermore,

data from December 23rd to December 31st are excluded to prevent distortions caused by the Christmas holiday season. The evaluations were conducted on a 64-bit Linux server equipped with dual Intel Xeon Gold 6226 CPUs, providing a total of 8 cores running at 2.7 GHz, and 288 GB of RAM. The core components of the column generation algorithm are implemented in C++, with each restricted linear master problem solved using HiGHS version 1.6.0 (Huangfu and Hall, 2018). Each instance was subject to a time limit. If the column generation reaches this limit before converging, it enters the search phase: the path with the largest fractional value is fixed at 1, and this process is repeated until a feasible integer solution is found.

Table 5 summarizes the results across all instances with a tight 30-minute time limit, that captures the realities in the field. For context, the third column shows the total number of trip requests and the number of trips successfully fulfilled by the current Paratransit system. The current Paratransit system, which uses a heuristic algorithm provided by RouteMatch given predetermined shifts, typically requires hours to perform the scheduling process. On average, this system accommodates 80.75% of the total trip requests. In the table, the “objective” value represents the number of requests served in the final integer solution; “time (s)” denotes the total runtime in seconds for the entire algorithm until convergence or the time limit. The 30-minute time limit experiment is designed to assess the solution quality of the proposed AGGNNI-CG when required to operate within a much shorter time frame. The goal is to enhance both the planning process and the user experience by significantly reducing scheduling time compared to the current system.

Table 5: Performance Comparison Between the Proposed AGGNNI-CG and Alternative Approaches With 30-Minute Time Limit.

| instance | number of edges<br>in original graph | total trip requests<br>/ current system | Baseline-CG |          | RF-CG     |          | AGGNNI-CG |          |
|----------|--------------------------------------|---|-------------|----------|-----------|----------|-----------|----------|
|          |                                      |   | objective   | time (s) | objective | time (s) | objective | time (s) |
| 20191202 | 902,025                              | 475/365                                 | 380         | 1,800    | 414       | 1,552    | 437       | 1,534    |
| 20191203 | 853,314                              | 462/342                                 | 368         | 1,800    | 407       | 1,800    | 439       | 898      |
| 20191204 | 1,258,323                            | 561/450                                 | 427         | 1,800    | 458       | 1,800    | 470       | 1,800    |
| 20191205 | 1,060,385                            | 515/409                                 | 387         | 1,800    | 442       | 1,795    | 480       | 1,737    |
| 20191206 | 1,035,815                            | 509/391                                 | 401         | 1,800    | 444       | 1,653    | 460       | 1,241    |
| 20191209 | 971,703                              | 493/427                                 | 380         | 1,800    | 406       | 1,800    | 461       | 1,594    |
| 20191210 | 1,031,748                            | 508/419                                 | 418         | 1,800    | 463       | 1,469    | 478       | 1,571    |
| 20191211 | 1,205,055                            | 549/443                                 | 418         | 1,800    | 501       | 1,800    | 450       | 1,800    |
| 20191212 | 1,023,638                            | 506/421                                 | 386         | 1,800    | 450       | 1,800    | 435       | 1,800    |
| 20191213 | 1,043,973                            | 511/398                                 | 394         | 1,800    | 423       | 1,800    | 479       | 1,231    |
| 20191216 | 913,458                              | 478/405                                 | 387         | 1,800    | 431       | 1,123    | 440       | 1,195    |
| 20191217 | 831,288                              | 456/405                                 | 436         | 1,793    | 410       | 908      | 435       | 986      |
| 20191218 | 898,230                              | 474/384                                 | 374         | 1,800    | 413       | 1,658    | 442       | 1,491    |
| 20191219 | 1,072,778                            | 518/443                                 | 402         | 1,800    | 467       | 1,800    | 483       | 1,415    |
| 20191220 | 987,539                              | 497/363                                 | 408         | 1,800    | 451       | 1,558    | 456       | 1,397    |
| average  | 1,005,952                            | 501/404                                 | 398         | 1,800    | 439       | 1,621    | 456       | 1,446    |

Table 5 shows that Baseline-CG hits the 30-minute time limit for almost all instances. This is expected as Baseline-CG needs much longer time to complete the pricing subproblems, thus struggling to explore sufficient number of high-quality paths for the master problem. This results in an average objective even worse than that of the existing system. In comparison, both RF-CG and AGGNNI-CG operate on reduced graph sizes, this accelerating the pricing subproblems. They improve solution quality by 10.3% and 14.6%, respectively, and reduce runtimes by 9.9% and 19.7%, respectively, compared to Baseline-CG. The improvement of RF-CG over Baseline-CG is in tune with the results reported in Morabit et al. (2023).

Table 5 also indicates that AGGNNI-CG provides significant advantage over RF-CG. On the one hand,

AGGNNI-CG achieves a 10% additional reduction in runtimes and it reaches the time limit on the three instances fewer than RF-CF. On the other hand, AGGNNI-CG improves the objective by 3.9% in average compared to RF-CF, and always improves the solution quality over the current system. This contrasts with RF-CG that may fail to improve over the current system (e.g., instance 20191209). These observations align with the classification results, as the GNN is able to identify promising edges more accurately than RF.

To further illustrate of the benefits of AGGNNI-CG, Table 6 presents a comparison of performance metrics when the time limit is extended to 1 hour. In this case, neither RF-CG nor AGGNNI-CG exceed time limit for any instance, whereas Baseline-CG continues to reach the time limit in 5 instances. With the extended run time, all three CG approaches show an increase in average objective values compared to the 30-minute time limit as expected. Baseline-CG, in particular, shows the most significant improvement, as it is the most affected by the 30-minute time limit bottleneck. As a result, RF-CG loses its solution quality advantage over Baseline-CG, now trailing by an average of 3.3%. In contrast, AGGNNI-CG maintains a 1% advantage in average objective value while achieving a remarkable 49.8% reduction in run time.

Table 6: Performance Comparison Between the Proposed AGGNNI-CG and Alternative Approaches With 1-Hour Time Limit.

| instance | Baseline-CG |          | RF-CG     |          | AGGNNI-CG |          |
|----------|-------------|----------|-----------|----------|-----------|----------|
|          | objective   | time (s) | objective | time (s) | objective | time (s) |
| 20191202 | 407         | 3,600    | 414       | 1,552    | 437       | 1,534    |
| 20191203 | 450         | 1,999    | 405       | 1,855    | 439       | 898      |
| 20191204 | 463         | 3,600    | 517       | 2,288    | 519       | 2,526    |
| 20191205 | 493         | 2,576    | 442       | 1,795    | 480       | 1,737    |
| 20191206 | 473         | 2,543    | 444       | 1,653    | 460       | 1,241    |
| 20191209 | 433         | 3,600    | 431       | 2,133    | 461       | 1,594    |
| 20191210 | 479         | 3,335    | 463       | 1,469    | 478       | 1,571    |
| 20191211 | 472         | 3,600    | 498       | 1,953    | 508       | 1,871    |
| 20191212 | 454         | 3,600    | 459       | 1,900    | 478       | 1,824    |
| 20191213 | 484         | 3,000    | 456       | 2,254    | 479       | 1,231    |
| 20191216 | 449         | 2,820    | 431       | 1,123    | 440       | 1,195    |
| 20191217 | 436         | 1,793    | 410       | 908      | 435       | 986      |
| 20191218 | 449         | 3,280    | 413       | 1,658    | 442       | 1,491    |
| 20191219 | 499         | 3,170    | 463       | 1,984    | 483       | 1,415    |
| 20191220 | 477         | 2,331    | 451       | 1,558    | 456       | 1,397    |
| average  | 461         | 2,993    | 446       | 1,739    | 466       | 1,501    |

In conclusion, the combination of improved solution quality and reduced computational time demonstrates the benefits and robustness of AGGNNI-CG. This is especially valuable for large-scale instances with high demand variability, making AGGNNI-CG highly suitable for real-world applications where both solution quality and computational efficiency are critical.

## 5.5 Sensitivity Analysis

This section presents a sensitivity analysis of the impact of different reduced graph configurations used in GNN training (RGTrn) and testing (RGTst). For each training instance, the RGTrn graphs provide the GNN-based model with labels indicating promising edges for learning. The quality of these graphs directly impacts the GNN ability to accurately identify promising edges. During testing, the RGTst graphs determine the reduced graph on which the column generation algorithm runs. The size of the RGTst graph represents a trade-off between solution quality and computation time in the column generation process.

Figure 16 summarizes the results of the proposed AGGNNI-CG when trained and tested with various types of RGTrn and RGTst graphs and the 1-hour time limit. The figure is organized into five groups, corresponding to the five types of RGTrn graphs. Within each group, the results for sixteen types of RGTst graphs are presented. For example, the first bar in Figure 16 represents the result of using RGTrn-A as the training graph and RGTst-2 as the test graph. The height of each bar indicates the average solution quality, while the height of the orange section reflects the average solution time for all test instances. The labels of vertical axis on the left and the right of the figure provide the scale in terms of solution quality and runtime, respectively.

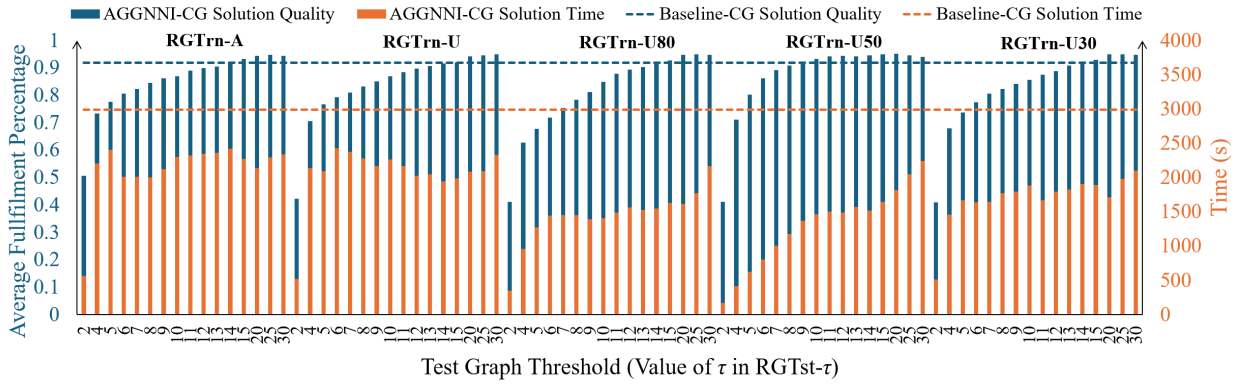


Figure 16: AGGNNI-CG Performance Comparison Across Different Types of RGTrn and RGTst Graphs, with Dashed Lines Representing Baseline-CG Metrics and Solid Lines Representing AGGNNI-CG Metrics.

To ensure a consistent comparison across different test days, which have varying numbers of trip requests, we calculate the fulfillment percentage (i.e., the ratio of trips fulfilled to total trip requests) for each day, and average this across all days to represent solution quality. Additionally, the average solution quality (blue dashed line) and solution time (orange dashed line) of Baseline-CG with 1-hour time limit are included for reference. The following key findings emerge from the sensitivity analysis in Figure 16:

**Impact of Training Graphs (RGTrn):** There is a clear distinction among the five training graph groups. The average solution times for RGTrn-A and RGTrn-U are higher than those of the remaining three groups. This suggests that edges selectively derived from paths with positive usage in solving the RLMP, rather than from all paths explored during the column generation iterations, are more suitable to be labeled as promising for supervised learning. Additionally, AGGNNI-CG exhibit high robustness, showing consistent performance across different RGTrn scales (e.g., RGTrn-U80, RGTrn-U50, and RGTrn-U30).

**Effect of Test Graphs (RGTst):** In terms of solution quality, smaller RGTst graphs (e.g., RGTst-2 and RGTst-4) generally result in faster solution times but at the expense of lower fulfillment percentages. As the scale of the RGTst graph increases, the solution quality improves, but this comes with longer computation times. A more balanced combination of solution quality and time is observed in mid-range RGTst graphs (e.g., between RGTst-10 and RGTst-15), where the solution quality approaches or even exceeds that of Baseline-CG, while the solution time is significantly reduced.

**Comparison with Baseline-CG Performance:** Across all RGTrn types, the proposed AGGNNI-CG consistently achieves a higher average fulfillment percentage than Baseline-CG, while drastically reducing

the solution time. This demonstrates the efficiency of the GNN-based graph reduction approach. Particularly for RGTrn-U80, RGTrn-U50 and RGTrn-U30, the combination of solution quality and solution time shows a substantial improvement over Baseline-CG, making these configurations highly suitable for practical applications.

In summary, the sensitivity analysis confirms that the proposed AGGNNI-CG is robust to variations in the scale of training graphs and achieves a desirable balance between solution quality and time for mid-scale test graphs. These results suggest that AGGNNI-CG is well-suited for large-scale, real-world JRPCSSP problems, where both computational efficiency and solution accuracy are critical.

## 6 Conclusions

This paper introduced the Joint Rider Trip Planning and Crew Shift Scheduling Problem (JRPCSSP) to avoid separating two important components of various mobility systems. Moreover, to meet the computational challenges of JRPCSSP, the paper proposed a novel solution method, called Attention and Gated GNN-Informed Column Generation (AGGNNI-CG) that hybridizes column generation and machine learning. The key idea underlying AGGNNI-CG is to reduce the size of the graphs explored by the pricing subproblems by only exploring promising edges, accelerating the most time-consuming component of the column generation. These edges are obtained by supervised learning, using a novel graph neural network that features both a multi-head attention mechanism and a gated architecture. The proposed GNN is ideally suited to cater for the different input sizes encountered during daily operations, where the number of requests, their locations, and request times vary from day to day.

The benefits of AGGNNI-CG was demonstrated on a real-world paratransit systems, where it was able to condense the graphs for the pricing subproblems by an order of magnitude. This led to a significant acceleration of the conventional column generation process. For complex instances where traditional column generation methods falter, AGGNNI-CG successfully delivers high-quality solutions within a practical time-frame. The methodology underlying AGGNNI-CG is also general and should apply to other applications as well.

There are several avenues for expanding upon this research. First, while this study leverages a reservation-based on-demand travel system for performance validation, it would be highly interesting to apply a similar approach to real-world multimodal transit systems. Second, it would be interesting to determine whether it is possible to generalize AGGNNI-CG to handle seamlessly both weekdays, weekends, and holidays, simplifying the deployment in practice. Third, extending the framework to support online rescheduling would address operational stochasticity in transportation systems. This would require incorporating real-time data streams to dynamically adjust schedules in response to disruptions like traffic congestion, vehicle breakdowns, and passenger no-shows.

## Declaration of generative AI and AI-assisted technologies in the writing process

During the preparation of this work the authors used ChatGPT in order to improve readability. After using this service, the authors reviewed and edited the content as needed and take full responsibility for the content of the publication.

## A Column Generation Details

For the completeness of this paper, this section provides the pseudocode of the column generation algorithm proposed in Section 3.

### A.1 Column Generation Outer Loop

Algorithm 1 outlines a branching heuristic to solve an integer programming formulation for JRTPCSSP. The goal is to iteratively construct an integral feasible solution  $\lambda$  by solving a series of restricted master problems with dynamically added columns and branching on fractional solutions.

---

**Algorithm 1:** Column Generation Outer Loop (Branching Heuristic in Section 3.3)

---

**Input :** Set of trip requests  $R$ , Fleet  $F$ , Set of driver shift candidates  $\Phi$ ,  
 Graph  $g = (N^g, E^g)$  with travel time  $t_{ij}$  associated with each edge  $(i, j) \in E^g$   
**Output:** An integer feasible solution  $\lambda$

```

1  $\Omega' \leftarrow \emptyset$ ;
2  $\lambda \leftarrow \text{None}$ ;
3  $\text{fixed\_columns} \leftarrow \emptyset$ ;
4 while  $\lambda$  is None do
5    $\lambda' \leftarrow \text{ColumnGenerationFixed}(\Omega', R, F, \Phi, \text{fixed\_columns}, g)$ ;
6   if  $\lambda'$  is integer then
7      $\lambda \leftarrow \lambda'$ ;
8     break;
9    $\theta_{\text{fix}} \leftarrow \text{FindMaxFractionalColumn}(\lambda')$ ;
10   $\text{fixed\_columns} \leftarrow \text{fixed\_columns} \cup \{\theta_{\text{fix}}\}$ ;
11 return  $\lambda$ ;

```

---

Lines 1–3 initialize the algorithm. The fixed columns set is used to record branching decisions, where specific columns are constrained to be 1 in subsequent iterations. Lines 4–10 form the core iterative loop. In each iteration, the algorithm finds new columns through the `ColumnGenerationFixed` procedure using the current problem state and fixed columns. If the resulting solution  $\lambda'$  is integer, it is assigned to  $\lambda$  and the algorithm terminates. Otherwise, the largest fractional column  $\theta_{\text{fix}}$  is identified using the `FindMaxFractionalColumn` routine, and this column is added to the set of fixed columns to guide the next iteration. Line 11 returns the final integer feasible solution  $\lambda$  once the loop has converged.

### A.2 Column Generation with Fixed Columns

Algorithm 2 describes the inner loop of the column generation procedure, which solves a restricted linear master problem (RLMP) iteratively while incorporating a fixed set of columns due to branching constraints. The algorithm starts with an initial set of columns  $\Omega'$  and repeatedly solves the RLMP using these columns and the current set of fixed variables. The RLMP solution returns dual variables associated with the trip constraints and resource constraints.

Lines 1–2 initialize the iterative process. In each iteration, the RLMP is solved with the current column pool  $\Omega'$  and the fixed column constraints, yielding a primal solution  $\lambda'$  and associated dual variables. Lines 4–6 loop over all shift candidates in  $\Phi$  and solve the pricing subproblem for each shift  $\phi$ , using the current dual variables to identify columns with negative reduced cost. Any generated columns are added to the set  $C_{\text{new}}$ .

---

**Algorithm 2:** Column Generation with Fixed Columns [ColumnGenerationFixed]

---

**Input** : Current set of columns  $\Omega'$ , Set of trip requests  $R$ , Fleet  $F$ , Set of driver shift candidates  $\Phi$ , Set of fixed columns  $fixed\_columns$ , Graph  $g = (N^g, E^g)$

**Output:** RLMP solution  $\lambda'$

```

1 while True do
2    $\lambda', \{\pi'_r\}_{r \in R}, \sigma' \leftarrow \text{SolveRLMP}(\Omega', fixed\_columns, R, F)$  ; // Solve the RLMP (Figure 4) with
    columns  $\Omega'$  and additional constraints on  $fixed\_columns$ 
3    $\mathcal{C}_{new} \leftarrow \emptyset$ ;
4   for  $\phi = (dr_s, dr_e) \in \Phi$  do
5      $\mathcal{C}_\phi \leftarrow \text{SolvePricing}(\{\pi'_r\}_{r \in R}, \sigma', \phi, g)$ ;
6      $\mathcal{C}_{new} \leftarrow \mathcal{C}_{new} \cup \mathcal{C}_\phi$ ;
7   if  $\mathcal{C}_{new} = \emptyset$  then
8     return  $\lambda'$  ; // Terminate when the Pricing Subproblem yields no new columns
9    $\Omega' \leftarrow \Omega' \cup \mathcal{C}_{new}$ ;

```

---

If no new columns are generated in an iteration, as checked in line 7, the algorithm terminates and returns the current RLMP solution  $\lambda'$ . Otherwise, line 9 updates the column set  $\Omega'$  by including the new columns, and the process repeats until optimality or time limit is reached.

### A.3 Solving the Pricing Subproblem

Algorithm 3 solves the pricing subproblem for a given driver shift  $\phi$  by identifying columns with negative reduced cost. It employs a dynamic programming algorithm on a graph (an original or a reduced graph in this study), where each label represents a partial route that originates at the depot and terminates at a specific node. A label is defined as  $L = (i, c, O, Re, S, t_a, t_s, t_d, prev)$ , where  $i$  denotes the current node,  $c$  is the reduced cost of the partial path,  $O$  is the set of open trip requests (i.e., requests that have been picked up but not yet dropped off),  $Re$  is the set of reachable trip requests, and  $S$  is the set of already served requests. The variables  $t_a$ ,  $t_s$ , and  $t_d$  represent the arrival, service start, and departure times at node  $i$ , respectively. These label components collectively track the consumption of resources (time, capacity) and ensure that constraints (1c) - (1k) are satisfied during path construction. The field  $prev$  stores a reference to the preceding label in the route, enabling backtracking to reconstruct complete paths.

Lines 1–4 initialize key data structures, including the priority queue  $L_{pool}$ , a processed label pool for each node, and the output set of columns  $Columns\_Found$ . Line 5 creates the initial label at the start depot and inserts it into the queue. Lines 6–8 define the main loop, which continues until the queue is empty or a predefined number of columns have been found. At each iteration, the label with the lowest cost is extracted and extended via the **LabelExtension** function (line 9). If the label reaches the destination depot (line 10), a feasible route is reconstructed using **BacktraceRoute**, and the resulting column is added to the solution set (lines 11–13). The loop terminates early if the maximum number of columns is reached.

If the current label does not reach the destination depot, lines 15–28 perform dominance checks to reduce the number of stored labels. A label  $L'$  is compared against previously processed labels at the same node to detect dominance relationships. If  $L'$  is dominated, it is skipped; if it dominates others, those are marked for removal. The surviving label is added to the processed set, and the label pool is updated. If the number of labels at a node exceeds a predefined limit, the labels with the highest cost are pruned.

Lines 29–31 define the dominance-checking procedure used above. A label  $L'$  is considered dominated by another label  $L''$  if  $L''$  arrives earlier, has lower cost, and represents a superset of visited requests.

---

**Algorithm 3:** Solve the Pricing Subproblem (Section 3.2) [SolvePricing]

---

**Input** : Dual variables  $\{\pi_r\}_{r \in R}$  (requests) and  $\sigma$  (fleet size), Driver shift  $\phi = (dr_s, dr_e)$ , Graph  $g = (N^g, E^g)$

**Output:** Set of new columns  $\mathcal{C}_\phi$  with negative reduced cost for shift  $\phi$

- 1  $L_{pool} \leftarrow$  Empty priority queue ordered by reduced cost;
- 2  $Processed\_Labels_i \leftarrow \emptyset$  for every node  $i \in N^g$ ;
- 3  $Columns\_Found \leftarrow \emptyset$ ;
- 4  $max\_columns \leftarrow$  predefined limit;
- 5  $max\_labels\_per\_node \leftarrow$  predefined limit;
- 6  $L_0 \leftarrow (i = 0, c = -\sigma, O = \emptyset, Re = P, S = \emptyset, t_a = dr_s, t_s = dr_s, t_d = dr_s, prev = \emptyset)$ ;
- 7  $L_{pool}.\text{Insert}(L_0)$ ;
- 8  $Processed\_Labels_0 \leftarrow Processed\_Labels_0 \cup \{L_0\}$ ;
- 9 **while** ( $L_{pool}$  is not empty)  $\wedge (|Columns\_Found| < max\_columns)$  **do**
- 10      $L = (i, c, O, Re, S, t_a, t_s, t_d, prev) \leftarrow L_{pool}.\text{ExtractMin}()$ ; // label with the lowest cost
- 11      $Generated\_Labels \leftarrow \text{LabelExtension}(L, \{\pi_r\}_{r \in R}, \phi, g)$ ;
- 12     **for**  $L' = (j, c', O', Re', S', t'_a, t'_s, t'_d, prev') \in Generated\_Labels$  **do**
- 13         **if**  $j = 2n + 1$  **then**
- 14              $\theta \leftarrow \text{BacktraceRoute}(L')$ ; // Backtrace route upon reaching destination depot
- 15              $Columns\_Found \leftarrow Columns\_Found \cup \{\theta\}$ ;
- 16             **if**  $|Columns\_Found| \geq max\_columns$  **then**
- 17                 **break**;
- 18         **else**
- 19              $dominated \leftarrow \text{False}$ ;
- 20              $Labels\_to\_Remove \leftarrow \emptyset$ ;
- 21             **for**  $L'' \in Processed\_Labels_j$  **do**
- 22                 **if**  $\text{CheckDominance}(L', L'')$  **then**
- 23                      $dominated \leftarrow \text{True}$ ; **break**;
- 24                 **if**  $\text{CheckDominance}(L'', L')$  **then**
- 25                      $Labels\_to\_Remove \leftarrow Labels\_to\_Remove \cup \{L''\}$ ; // Remove  $L''$  if dominated by  $L'$
- 26         **if**  $dominated = \text{True}$  **then**
- 27             **continue**; // Skip if  $L'$  is dominated by any  $L'' \in Processed\_Labels_j$
- 28      $Processed\_Labels_j \leftarrow Processed\_Labels_j \setminus Labels\_to\_Remove$ ;
- 29      $L_{pool}.\text{Insert}(L')$ ;
- 30      $Processed\_Labels_j \leftarrow Processed\_Labels_j \cup \{L'\}$ ;
- 31     **if**  $|Processed\_Labels_j| > max\_labels\_per\_node$  **then**
- 32         Remove label(s) with the highest cost from  $Processed\_Labels_j$ ;
- 33 **return**  $Columns\_Found$ ;
- 34 **Procedure**  $\text{CheckDominance}(L', L'')$
- 35     Let  $L' = (j, c', O', Re', S', t'_a, t'_s, t'_d)$ ;
- 36     Let  $L'' = (j, c'', O'', Re'', S'', t''_a, t''_s, t''_d)$ ;
- 37      $dominated \leftarrow (O'' \subseteq O') \wedge (t''_d \leq t'_d) \wedge (c'' \leq c') \wedge (|S''| \geq |S'|)$ ; //  $L'$  dominated by  $L''$
- 38     **return**  $dominated$ ;

---

#### A.4 Label Extension Details

Algorithm 4 implements the label extension procedure used within the pricing subproblem. Given a current label  $L = (i, c, O, Re, S, t_a, t_s, t_d, prev)$ , the algorithm generates feasible extensions by considering depot

returns, drop-off actions, and pickup opportunities for unserved trip requests. Each extension results in a new label, which is added to the set of generated labels if it satisfies temporal and feasibility constraints.

---

**Algorithm 4:** Label Extension [LabelExtension]

---

**Input** : Current Label  $L = (i, c, O, Re, S, t_a, t_s, t_d, prev)$ , Dual variables  $\{\pi_r\}_{r \in R}$ , Driver shift  $\phi = (dr_s, dr_e)$ , Graph  $g = (N^g, E^g)$

**Output:** Set of extended labels *Generated\_Labels*

```

1 Generated_Labels  $\leftarrow \emptyset$ ;
2 if  $(i \neq 0) \wedge (|O| = 0) \wedge (c < 0)$  then
3    $j \leftarrow 2n + 1$ ; // Back to depot
4    $(t'_a, t'_s, t'_d) \leftarrow \text{TimeUpdate}(t_d, i, j)$ ;
5   if TimeFeasible $(t'_a, j, dr_e)$  then
6      $c' \leftarrow c; O' \leftarrow \emptyset; Re' \leftarrow \emptyset; S' \leftarrow S$ ;
7      $L' \leftarrow (j, c', O', Re', S', t'_a, t'_s, t'_d, prev' = L)$ ;
8     Generated_Labels  $\leftarrow \text{Generated_Labels} \cup \{L'\}$ ;
9 for  $r \in O$  do
10   $j \leftarrow n + r$ ; // Drop-off node  $n + r$  for request  $r$ 
11  if  $(i, j) \notin E^g$  then
12    continue
13   $(t'_a, t'_s, t'_d) \leftarrow \text{TimeUpdate}(t_d, i, j)$ ;
14  if TimeFeasible $(t'_a, j, dr_e)$  then
15     $c' \leftarrow c; O' \leftarrow O \setminus \{r\}; S' \leftarrow S; Re' \leftarrow \text{ReachableUpdate}(Re, j)$ ;
16     $L' \leftarrow (j, c', O', Re', S', t'_a, t'_s, t'_d, prev' = L)$ ;
17    Generated_Labels  $\leftarrow \text{Generated_Labels} \cup \{L'\}$ ;
18 for  $r \in Re$  do
19   $j \leftarrow r$ ; // Pickup node  $r$  for request  $r$ 
20  if  $(i, j) \notin E^g$  then
21    continue
22  if  $(|O| < C) \wedge (r \notin O) \wedge (r \notin S)$  then
23     $(t'_a, t'_s, t'_d) \leftarrow \text{TimeUpdate}(t_d, i, j)$ ;
24    if TimeFeasible $(t'_a, j, dr_e)$  then
25       $c' \leftarrow c - \pi_r; O' \leftarrow O \cup \{r\}; S' \leftarrow S \cup \{r\}; Re' \leftarrow \text{ReachableUpdate}(Re, j)$ ;
26       $L' \leftarrow (j, c', O', Re', S', t'_a, t'_s, t'_d, prev' = L)$ ;
27      Generated_Labels  $\leftarrow \text{Generated_Labels} \cup \{L'\}$ ;
28 return Generated_Labels;
29 Procedure TimeUpdate $(t_d^{prev}, i, j)$ 
30   $t'_a = t_d^{prev} + t_{ij}; t'_s = \max\{t'_a, a_j\}; t'_d = t'_s + s_j$ ;
31  return  $(t'_a, t'_s, t'_d)$ ;
32 Procedure ReachableUpdate $(Re^{prev}, current\_node)$ 
33   $Re' \leftarrow \{r \in Re^{prev} \mid$ 
34     $\text{TimeFeasible}(current\_node, r) \wedge \text{TimeFeasible}(r, r + n) \wedge \text{TimeFeasible}(r + n, 2n + 1)\}$ ;
35  return  $Re'$ ;
36 Procedure TimeFeasible $(t'_a, j, dr_e)$ 
37  return  $(t'_a \leq b_j) \wedge (t'_a \leq dr_e)$ ;

```

---

Lines 1–8 handle the case where the route may return to the depot. If the label is not at the depot and has no open requests, and the reduced cost is negative, a depot return is considered. The algorithm computes updated timing information and checks time feasibility before appending the corresponding extended label.

Lines 9–17 iterate over all served requests to evaluate drop-off possibilities. For each request  $r$ , the corresponding drop-off node  $j = n + r$  is checked for edge existence and temporal feasibility. If feasible, a new label is generated with updated cost, state sets, and reachable request sets.

Lines 18–27 focus on pickup actions for all reachable trip requests. For each candidate  $r \in Re$ , the pickup node is evaluated under precedence and capacity constraints (e.g., the number of open requests must be below vehicle capacity, and a request cannot be picked up again if already served). If all feasibility conditions are satisfied, a new label is constructed with the updated attributes and added to the output.

The subprocedures at the end define utility functions. **TimeUpdate** (lines 29–31) computes updated arrival, service, and departure times. **ReachableUpdate** (lines 32–34) filters reachable requests based on temporal feasibility from the new node. Finally, **TimeFeasible** (lines 35–36) checks whether a proposed arrival time is within the time window of the target node.

## B Feature Importance Analysis

To evaluate the relative importance of features used in the GNN model, this paper extends existing feature importance methods for GNNs. To the author’s knowledge, current methods like GNNExplainer (Ying et al., 2019) only support importance ranking for node features. To address this limitation, this paper enhances the GNNExplainer framework to incorporate edge feature masking alongside node feature masking.

Table 7 introduces the notations used in the enhanced GNNExplainer. The following augmented loss function that integrates edge feature masking is proposed:

$$\mathcal{L}_{\text{enhanced}} = \mathcal{L}_{\text{pred}}(\hat{y}, y) + \mathcal{L}_{\text{node}} + \mathcal{L}_{\text{edge}}, \quad (16)$$

where

$$\begin{aligned} \mathcal{L}_{\text{edge}} = & \lambda_{\text{edge\_size}} \cdot \frac{1}{|B_{\text{edge}}|} \sum_{i \in B_{\text{edge}}} \sigma(M_{\text{edge}}[i]) \\ & + \lambda_{\text{edge\_ent}} \cdot \frac{1}{|B_{\text{edge}}|} \sum_{i \in B_{\text{edge}}} H(\sigma(M_{\text{edge}}[i])), \end{aligned} \quad (17)$$

$$\begin{aligned} \mathcal{L}_{\text{node}} = & \lambda_{\text{node\_size}} \cdot \frac{1}{|B_{\text{node}}|} \sum_{i \in B_{\text{node}}} \sigma(M_{\text{node}}[i]) \\ & + \lambda_{\text{node\_ent}} \cdot \frac{1}{|B_{\text{node}}|} \sum_{i \in B_{\text{node}}} H(\sigma(M_{\text{node}}[i])), \end{aligned} \quad (18)$$

$$\mathcal{L}_{\text{pred}} = - \sum_i [y_i \log(\hat{y}_i) + (1 - y_i) \log(1 - \hat{y}_i)], \quad (19)$$

$$H(p) = -p \log(p + \epsilon) - (1 - p) \log(1 - p + \epsilon). \quad (20)$$

### B.1 Feature Importance Results and Implications

To determine the final importance score for each feature, the learned mask values across all nodes/edges were averaged and then summed across the 15 test instances. Figure 17 presents the ranking of feature importance in the GNN model.

Table 7: Enhanced GNNExplainer loss function parameters

| Symbol                        | Definition  | Value      |
|-------------------------------|---|------------|
| $M_{\text{node}}$             | Learnable node feature importance parameters                  | -          |
| $M_{\text{edge}}$             | Learnable edge feature importance parameters                  | -          |
| $B_{\text{node}}$             | Boolean mask indicating node features with non-zero gradients | -          |
| $B_{\text{edge}}$             | Boolean mask indicating edge features with non-zero gradients | -          |
| $\sigma(\cdot)$               | Sigmoid function  | -          |
| $\lambda_{\text{node\_size}}$ | Node sparsity coefficient                                     | 1.0        |
| $\lambda_{\text{node\_ent}}$  | Node entropy coefficient                                      | 0.1        |
| $\lambda_{\text{edge\_size}}$ | Edge sparsity coefficient                                     | 1.0        |
| $\lambda_{\text{edge\_ent}}$  | Edge entropy coefficient                                      | 0.1        |
| $\epsilon$                    | Numerical stability constant                                  | $10^{-15}$ |

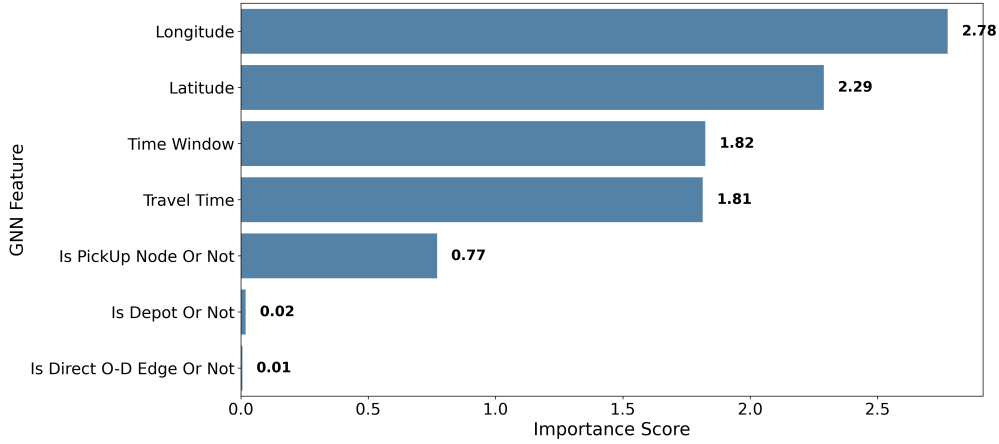


Figure 17: Feature Importance on the GNN Model

The analysis reveals that spatial information, specifically the geographic coordinates, contributes most significantly to the model's performance. Longitude (2.78) and latitude (2.29) attained the highest importance scores, highlighting the fundamental role of spatial positioning in transportation routing decisions. Time window constraints (1.82) and travel time (1.81) follow closely with nearly identical importance scores, demonstrating the complementary influence of temporal features on the GNN model.

## References

Akiba, T., Sano, S., Yanase, T., Ohta, T., Koyama, M., 2019. Optuna: A next-generation hyperparameter optimization framework, in: Proceedings of the 25th ACM SIGKDD international conference on knowledge discovery & data mining, 2623–2631.

Amberg, B., Amberg, B., Kliewer, N., 2019. Robust efficiency in urban public transportation: Minimizing delay propagation in cost-efficient bus and driver schedules. *Transportation Science* 53, 89–112.

Andrade-Michel, A., Ríos-Solís, Y.A., Boyer, V., 2021. Vehicle and reliable driver scheduling for public bus transportation systems. *Transportation Research Part B: Methodological* 145, 290–301.

Bengio, Y., Lodi, A., Prouvost, A., 2021. Machine learning for combinatorial optimization: a methodological tour d’horizon. *European Journal of Operational Research* 290, 405–421.

Borndörfer, R., Schulz, C., Seidl, S., Weider, S., 2017. Integration of duty scheduling and rostering to increase driver satisfaction. *Public Transport* 9, 177–191.

Braekers, K., Caris, A., Janssens, G.K., 2014. Exact and meta-heuristic approach for a general heterogeneous dial-a-ride problem with multiple depots. *Transportation Research Part B: Methodological* 67, 166–186.

Bresson, X., Laurent, T., 2017. Residual gated graph convnets. arXiv preprint arXiv:1711.07553.

Brody, S., Alon, U., Yahav, E., 2021. How attentive are graph attention networks? arXiv preprint arXiv:2105.14491.

Cordeau, J.F., 2006. A branch-and-cut algorithm for the dial-a-ride problem. *Operations Research* 54, 573–586.

Cordeau, J.F., Laporte, G., 2003. A tabu search heuristic for the static multi-vehicle dial-a-ride problem. *Transportation Research Part B: Methodological* 37, 579–594.

Cordeau, J.F., Laporte, G., 2007. The dial-a-ride problem: models and algorithms. *Annals of operations research* 153, 29–46.

Cordeau, Jean-Francois and Groupe d’études et de recherche en analyse des décisions (Montréal, Québec), 2000. The VRP with time windows. Citeseer.

Cubillos, C., Urra, E., Rodríguez, N., 2009. Application of genetic algorithms for the darptw problem. *International Journal of Computers Communications & Control* 4, 127–136.

Feng, T., Lusby, R.M., Zhang, Y., Tao, S., Zhang, B., Peng, Q., 2024. A branch-and-price algorithm for integrating urban rail crew scheduling and rostering problems. *Transportation Research Part B: Methodological* 183, 102941.

Garaix, T., Artigues, C., Feillet, D., Josselin, D., 2010. Vehicle routing problems with alternative paths: An application to on-demand transportation. *European Journal of Operational Research* 204, 62–75.

Garaix, T., Artigues, C., Feillet, D., Josselin, D., 2011. Optimization of occupancy rate in dial-a-ride problems via linear fractional column generation. *Computers & Operations Research* 38, 1435–1442.

Gschwind, T., Drexel, M., 2019. Adaptive large neighborhood search with a constant-time feasibility test for the dial-a-ride problem. *Transportation Science* 53, 480–491.

Gschwind, T., Irnich, S., 2015. Effective handling of dynamic time windows and its application to solving the dial-a-ride problem. *Transportation Science* 49, 335–354.

Ho, S.C., Szeto, W.Y., Kuo, Y.H., Leung, J.M., Petering, M., Tou, T.W., 2018. A survey of dial-a-ride problems: Literature review and recent developments. *Transportation Research Part B: Methodological* 111, 395–421.

Huangfu, Q., Hall, J.J., 2018. Parallelizing the dual revised simplex method. *Mathematical Programming Computation* 10, 119–142.

Jain, S., Hentenryck, P.V., 2011. Large neighborhood search for dial-a-ride problems, in: Lee, J.H. (Ed.), *Principles and Practice of Constraint Programming - CP 2011 - 17th International Conference, CP 2011, Perugia, Italy, September 12-16, 2011. Proceedings*, Springer. 400–413. [10.1007/978-3-642-23786-7\\_31](https://doi.org/10.1007/978-3-642-23786-7_31).

Jorgensen, R.M., Larsen, J., Bergvinsdottir, K.B., 2007. Solving the dial-a-ride problem using genetic algorithms. *Journal of the operational research society* 58, 1321–1331.

Joshi, C.K., Laurent, T., Bresson, X., 2019. An efficient graph convolutional network technique for the travelling salesman problem. *arXiv preprint arXiv:1906.01227*.

Kang, L., Chen, S., Meng, Q., 2019. Bus and driver scheduling with mealtime windows for a single public bus route. *Transportation Research Part C: Emerging Technologies* 101, 145–160.

Karimi-Mamaghan, M., Mohammadi, M., Meyer, P., Karimi-Mamaghan, A.M., Talbi, E.G., 2022. Machine learning at the service of meta-heuristics for solving combinatorial optimization problems: A state-of-the-art. *European Journal of Operational Research* 296, 393–422.

Kingma, D.P., Ba, J., 2014. Adam: A method for stochastic optimization. *arXiv preprint arXiv:1412.6980*.

Kipf, T.N., Welling, M., 2016. Semi-supervised classification with graph convolutional networks. *arXiv preprint arXiv:1609.02907*.

Kirchler, D., Calvo, R.W., 2013. A granular tabu search algorithm for the dial-a-ride problem. *Transportation Research Part B: Methodological* 56, 120–135.

Kotary, J., Fioretto, F., Van Hentenryck, P., Wilder, B., 2021. End-to-end constrained optimization learning: A survey. *arXiv preprint arXiv:2103.16378*.

Lu, J., Nie, Q., Mahmoudi, M., Ou, J., Li, C., Zhou, X.S., 2022. Rich arc routing problem in city logistics: Models and solution algorithms using a fluid queue-based time-dependent travel time representation. *Transportation Research Part B: Methodological* 166, 143–182.

Mazyavkina, N., Sviridov, S., Ivanov, S., Burnaev, E., 2021. Reinforcement learning for combinatorial optimization: A survey. *Computers & Operations Research* 134, 105400.

Morabit, M., Desaulniers, G., Lodi, A., 2021. Machine-learning-based column selection for column generation. *Transportation Science* 55, 815–831.

Morabit, M., Desaulniers, G., Lodi, A., 2023. Machine-learning-based arc selection for constrained shortest path problems in column generation. *INFORMS Journal on Optimization* 5, 191–210.

Nazari, M., Oroojlooy, A., Snyder, L., Takáć, M., 2018. Reinforcement learning for solving the vehicle routing problem. *Advances in neural information processing systems* 31.

Partnership for an Advanced Computing Environment (PACE), 2017. PACE - Partnership for an Advanced Computing Environment. [Online; accessed 18-December-2023].

Portugal, R., Lourenço, H.R., Paixão, J.P., 2009. Driver scheduling problem modelling. *Public Transport* 1, 103–120.

PyTorch-Geometric, 2024. Batching — pytorch geometric 2023 documentation. <https://pytorch-geometric.readthedocs.io/en/latest/advanced/batching.html>. Accessed: 2024-12-27.

Qu, Y., Bard, J.F., 2015. A branch-and-price-and-cut algorithm for heterogeneous pickup and delivery problems with configurable vehicle capacity. *Transportation Science* 49, 254–270.

Riley, C., Legrain, A., Van Hentenryck, P., 2019. Column generation for real-time ride-sharing operations, in: *Integration of Constraint Programming, Artificial Intelligence, and Operations Research: 16th International Conference, CPAIOR 2019, Thessaloniki, Greece, June 4–7, 2019, Proceedings* 16, Springer. 472–487.

Ropke, S., Cordeau, J.F., Laporte, G., 2007. Models and branch-and-cut algorithms for pickup and delivery problems with time windows. *Networks: An International Journal* 49, 258–272.

Ropke, S., Pisinger, D., 2006. An adaptive large neighborhood search heuristic for the pickup and delivery problem with time windows. *Transportation science* 40, 455–472.

Shen, Y., Sun, Y., Li, X., Eberhard, A., Ernst, A., 2022. Enhancing column generation by a machine-learning-based pricing heuristic for graph coloring, in: *Proceedings of the AAAI Conference on Artificial Intelligence*, 9926–9934.

Tóth, A., Krész, M., 2013. An efficient solution approach for real-world driver scheduling problems in urban bus transportation. *Central European Journal of Operations Research* 21, 75–94.

Toth, P., Vigo, D., 2014. *Vehicle routing: problems, methods, and applications*. SIAM.

Veličković, P., Cucurull, G., Casanova, A., Romero, A., Lio, P., Bengio, Y., 2017. Graph attention networks. *arXiv preprint arXiv:1710.10903*.

Vinyals, O., Fortunato, M., Jaitly, N., 2015. Pointer networks. *Advances in neural information processing systems* 28.

Wren, A., Wren, D.O., 1995. A genetic algorithm for public transport driver scheduling. *Computers & Operations Research* 22, 101–110.

Ying, Z., Bourgeois, D., You, J., Zitnik, M., Leskovec, J., 2019. Gnnexplainer: Generating explanations for graph neural networks. *Advances in neural information processing systems* 32.

Yuan, E., Chen, W., Hentenryck, P.V., 2022a. Reinforcement learning from optimization proxy for ride-hailing vehicle relocation. *J. Artif. Intell. Res.* 75, 985–1002. [10.1613/JAIR.1.13794](https://doi.org/10.1613/JAIR.1.13794).

Yuan, H., Jiang, P., Song, S., 2022b. The neural-prediction based acceleration algorithm of column generation for graph-based set covering problems, in: 2022 IEEE International Conference on Systems, Man, and Cybernetics (SMC), IEEE. 1115–1120.